

Oceanographic dataset of the near-shore water column of the northeastern Gulf of St. Lawrence, Canada, during the ice-free season

5 Emilie Arseneault^{1,2}, Neha Joshi^{2,3}, Julie Carrière⁴, Émilie Saulnier-Talbot^{1,2,3}

¹Biology Department, Université Laval, Québec, QC, G1V 0A6, Canada

²Québec-Océan and Institute of Integrative Biology and Systems, Université Laval, Québec, QC, G1V 0A6, Canada

³Geography Department, Université Laval, Québec, QC, G1V 0A6, Canada

10 ⁴Northern Institute for Research in Environment and Occupational Health and Safety (INREST), Sept-Îles, QC, G4R 2B2, Canada

Correspondence to: Emilie Arseneault (emilie.arseneault.3@ulaval.ca)

Abstract. Coastal ecosystems are highly dynamic and vulnerable to both climate changes and anthropogenic pressures. The Sept-Îles region, located in the northwestern Gulf of St. Lawrence, is a high-use subarctic coastal system with diverse urban, industrial and maritime activities. This study presents analyses of monthly water column profiles at 35 sites focusing on temperature, salinity and chlorophyll fluorescence, used as a proxy of phytoplankton biomass, during the ice-free season. Using a conductivity, temperature and depth (CTD) [sensorprobe](#), water column profiles were collected from May to October 2022 along the coastline, at sites between 2- and 52- meters depth. Results revealed a thermocline developing in spring, intensifying in summer and disappearing in autumn. Chlorophyll *a* (Chl *a*) concentrations peaked below the thermocline in July, while secondary increases were recorded at the surface in September, consistent with observations of an autumn bloom in similar environments. These findings highlight the complex dynamic of physical and biological [parameters-variables](#) in the coastal water column, and the importance of the timing of sampling to fully capture seasonal variability. To improve future research in the area, measuring nutrient concentrations would be essential for detecting potential upwelling events and better explaining phytoplankton variation during summer. This study provides a valuable baseline for future investigations and justifies the continuation of measurements of water column variability in the region, in the context of rapid climate change. The complete dataset is available via <https://doi.org/10.5683/SP3/ALRWON> (Arseneault & Saulnier-Talbot, 2025a).

1 Introduction

Coastal environments are at the forefront of climate change impacts, experiencing diverse types of alterations due to rising global temperatures and anthropogenic activities (IPCC, 2023). These changes are noticeable in the Gulf of St. Lawrence, where sea ice cover has declined markedly over the past decade (Galbraith et al., 2024a). This trend, linked to rising winter air temperatures over the past few decades, highlights the region's sensitivity to global warming, which is expected to lead to increasingly ice-free conditions in the near future (Galbraith et al., 2024a). The Sept-Îles region, located in the northwestern

Gulf of St. Lawrence, represents an economically vital area, hosting the most important mineral port in North America (PSI, 2025). Because of its industrial importance, the area is susceptible to several anthropogenic drivers (Beauchesne et al., 2020), in addition to rapid climatic changes. Among these, the disappearance of seasonal sea-ice is the most evident (Allard et al., 2025). In an effort to better understand the changing dynamics of the coastal ecosystem, several biodiversity studies are being conducted in the region's aquatic environment, covering diverse topics such as benthic communities (Dreujou et al., 2020; Joshi et al. 2025), intertidal and coastal diatoms (Arseneault et al., 2023; Arseneault & Saulnier-Talbot, 2025b), algal and bacterial pigments (Lefebvre, 2023; Araújo et al., 2022), microbial _{sed}DNA (Bélanger, 2024), and sea-ice ecology (Allard et al., 2025). Regular environmental monitoring has also been undertaken (Carrière et al., 2018a; Ferrario et al., 2022), and the Bay of Sept-Îles (BSI) is currently part of the Enviro-Actions program, allowing a near real-time monitoring of industrial port zones (Carrière and Dreujou, 2024). In this context, understanding the hydrological characteristics of the Sept-Îles region (Shaw et al., 2022) and the dynamics of the water column is crucial for tracking the variability, rate, direction and intensity of environmental change over time.

Among the most significant features of the water column, the thermocline, a water layer at which temperature decreases rapidly with depth, plays a key role in regulating stratification. This division of the water column into different layers can create barriers for organisms (Fiedler, 2010). Seasonal stratification regulates phytoplankton dynamics, with spring blooms commonly observed in temperate waters, including the BSI (Roden and Raine, 1994; Araújo et al., 2022; Lim et al., 2025). Most studies focusing on water column layers are usually carried out in deeper areas, far from the coast (de Boyer Montégut et al., 2004; Galbraith, 2006). However, evidence of stratified water columns in shallow coastal areas has also been documented. For example, on the west coast of Ireland, stratification within 10 km of the shore was observed (Roden and Raine, 1994) and in southern waters of Korea, thermal stratification was found to occur at sites between 5- and 30-m depths (Lim et al., 2025). Despite these findings, studies on shallow-water stratification remain scarce.

Given the combination of climatic and direct anthropogenic pressures in this region, ~~understanding-documenting baseline the~~ physical and biological ~~baseline~~-conditions ~~in the coastal water column of the aquatic environment~~ is essential for assessing potential ecological ~~at changes transformations~~ that could affect the food web and impact ecosystem services, such as fisheries and tourism. ~~Establishing this baseline is also important for future monitoring and management initiatives,~~ including the “Chaire de recherche sur les écosystèmes côtiers et les activités portuaires, industrielles et maritimes” (or EcoZone Chair, at Université Laval), which seeks to improve knowledge on coastal ecosystem functioning and to ensure sustainable management of these ecosystems subjected to urban, port, industrial and maritime activities.

~~The objective of this study was is study aimed~~ to characterize the ~~spatial and seasonal dynamics of the near-shore~~ water column ~~profiles~~ in the Sept-Îles region ~~by analyzing spatial and temporal variations in key oceanographic parameters~~ during the ice-free season. ~~We aimed to (1) describe monthly vertical profiles between May and October 2022, of temperature,~~

70 salinity, turbidity, and in vivo chlorophyll *a* fluorescence; (2) examine spatial and temporal patterns of these key
oceanographic parameters; and (3) identify thermocline structure and fluorescence patterns to better understand how
temperature and primary production co-vary in this region throughout the ice-free season. ~~By linking these observations to
broader environmental drivers, the results will serve as a baseline for understanding ongoing changes and support studies
aimed at monitoring and mitigating the effects of the various pressures in this coastal zone. The dataset generated in this
study also represents a valuable resource for future research and management initiatives as it can be reused for projects
related to coastal monitoring. Additionally, it contributes to initiatives such as the “Chaire de recherche sur les écosystèmes
côtiers et les activités portuaires, industrielles et maritimes” (or EcoZone Chair, at Université Laval), which seeks to improve
75 knowledge on coastal ecosystem functioning and to ensure sustainable management of these ecosystems subjected to port,
industrial and maritime activities.~~

80 ~~Water column profiles were collected once per month between May and October 2022, with a conductivity, temperature and
depth (CTD) sensor. We emphasized the description of temperature, salinity and fluorescence. The latter was used as an
indicator of phytoplankton biomass based on chlorophyll *a* (Chl *a*) concentrations recorded by the instrument. These profiles
provided valuable insights into the stratification and mixing dynamics that shape the physical environment of the region. The
main objectives of this study are to describe the water column profiles, and to analyze their spatial and temporal dynamics.
We also aim to investigate thermocline patterns and Chl *a* distribution to gain a better understanding of how temperature and
primary production co-vary in this region throughout the ice-free season.~~

85 **2 Material and methods**

2.1 Study area

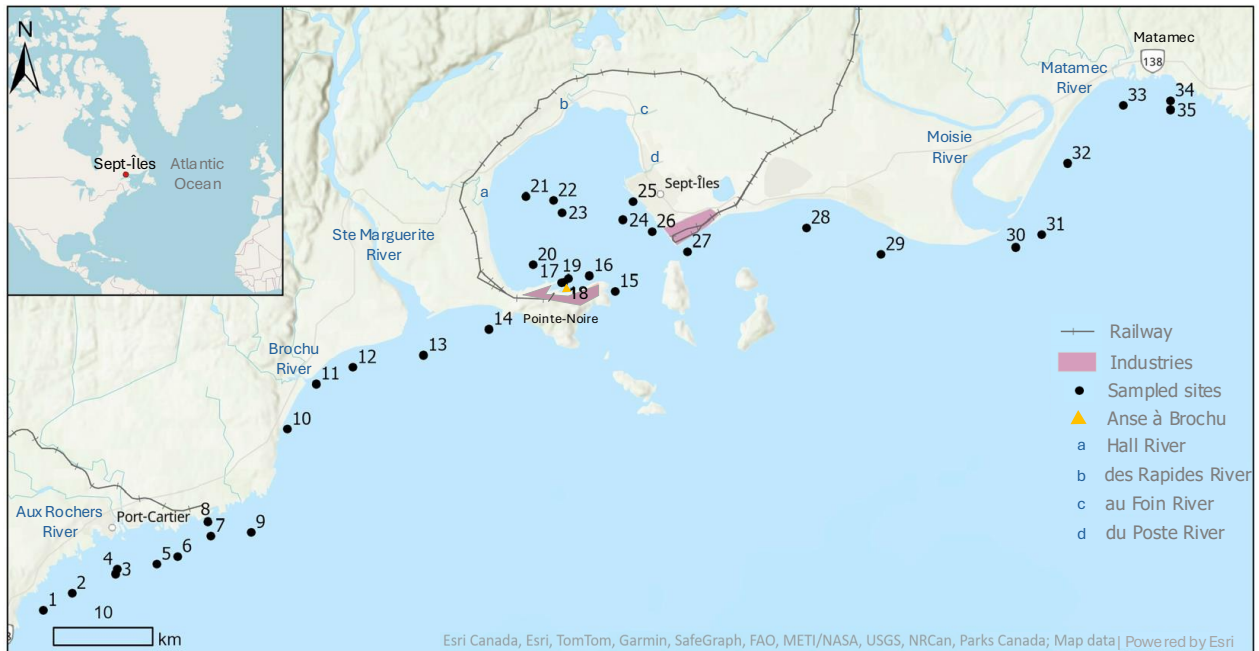


Figure 1: Map of the location of the 35 sites sampled around Sept-Îles and the major rivers of the region.

- 90 The study area covers the coastline of the Sept-Îles region, between 66°56' N and 65°54' W (Fig. 1). Situated in the northwestern Gulf of St. Lawrence, this region features a mix of saltwater brought by the Atlantic Ocean and freshwater from the St. Lawrence River and its tributaries (Lapointe, 2000; Carrière et al., 2018b). The region is under a semi-diurnal tidal system where tides range between 0.39 m to 3.6 m in Port-Cartier and 0.43 to 3.36 m in Sept-Îles (Fisheries and Ocean Canada, 2024). The area has a subarctic climate and has historically been covered by sea ice between November and April
- 95 (Aubut Demers et al., 2018). However, this period has been shrinking rapidly, and nearly ice-free winters could become more common due to climate warming (Galbraith et al., 2024a). Since 2010, the Gulf of St. Lawrence has experienced 4 winters with nearly ice-free conditions around the end of the season (Galbraith et al., 2024a).

- According to a study on the hydrodynamics of the BSI (Shaw et al., 2022), the area exhibits an estuarine circulation pattern.
- 100 Currents are seaward at the surface (2-10 meters) and shoreward in deeper waters (10-30 meters). Surface drifter measurements indicate average and maximum speeds of 17.4 cm s^{-1} and 86.6 cm s^{-1} , respectively. While locally dominated by tides, currents in the bay result from complex interactions between tides, estuarine circulation, winds, and the Earth's rotation. Water residence time is estimated to be 5.6 ± 3.5 days.

105 Diverse types of land-use along the transect were observed: natural coastlines with less developed areas, residential areas
(urban and suburban) and Industrial-Port (IP) Zones. Sites 5 to 8 in Port-Cartier are located in an IP zone, and the Port of
Sept-Îles (PSI) is the second largest Canadian port for annual activity (PSI, 2025) where several heavy industries contribute
to the economic importance of the region. The Matamec sector presents a less developed and more pristine environment,
featuring an ecological reserve and the Matamec River, which is of great conservation value (Government of Quebec, 2011).
110 The study area is affected by freshwater input from the Ste-Marguerite and Moisie rivers, damned and wild, respectively.
Smaller rivers also flow in the area, including the rivière aux Rochers in Port-Cartier and Brochu River, West of the Ste-
Marguerite. The Hall, des Rapides, aux Foins and du Poste rivers flow into the BSI, with around $22 \text{ m}^3 \text{ s}^{-1}$ of freshwater
input into this area annually (Shaw *et al.*, 2019).

2.2 Water sampling

115 ~~Water column~~The vertical profiles of temperature, salinity, turbidity, fluorescence, and photosynthetically active radiation
(PAR) were directly obtained with a measured using a Sea-Bird Electronics Conductivity-Temperature-Depth (CTD)
instrument probe equipped with sensors that measure temperature and salinity (Sea-Bird Electronics SBE19plusV2),
photosynthetically active radiation (PAR; Biospherical QSP-2300L with a spherical quantum sensor), turbidity (Seapoint)
and in vivo chlorophyll fluorescence (Seapoint). The sensors were last calibrated in 2017, so the data should be interpreted
120 with caution and considered as relative rather than absolute values. ~~two added Seapoint sensors, one for turbidity and one
for fluorometry (i.e., Chl *a*). The latter~~Fluorescence was used as an indicator of phytoplankton chlorophyll *a* biomass (Chl *a*).
~~biomass based on chlorophyll *a* (Chl *a*) concentrations recorded by the instrument.~~ Chl *a* is an indicator of phytoplankton
biomass and reflects the level of primary production in coastal waters (Araújo *et al.*, 2022). The CTD was equipped with an
integrated software system that automatically calculated practical salinity, density, specific volume anomaly, Brunt-
125 Väisälä frequency, Sigma-T, potential temperature, Sigma-Theta, freezing temperature, sound velocity, and absolute
salinity. At each site, the CTD was lowered to approximately 2-3 m above the seafloor to prevent potential damage to the
instrument and had an average descent speed of 1 m/s. Measurements along the transect were made monthly at all sites
between May and October 2022, (24th to 26th of May, 14th to 15th of June, 19th to 21st of July, 16th to 17th of August, 13th to
14th of September and 24th of October), except at site 34 in May and site 25 in June due to technical problems. The full
130 dataset is available at <https://doi.org/10.5683/SP3/ALRWON> (Arseneault & Saulnier-Talbot, 2025a). Meteorological data
for the week prior to sampling was also documented using data from the Government of Canada (2025) (Table A14). To
facilitate visualizations, the 35 sites were divided into three Zones (Table 1). Sites 1 to 15 between Port-Cartier and the west
of the BSI were defined as Zone 1, sites inside the BSI (16 to 27) were defined as Zone 2, and Zone 3 encompasses the sites
from the east of the BSI to Matamec (28 to 35). Monthly vertical profiles of temperature, salinity, turbidity and fluorescence
at each site were generated using “ggplot” (R core Team, 2022). With the same statistical package, relationships between
Chl *a* and

Table 1: Site zones, description of land use, and mean of the maximum CTD depth for each site (Zone 1 = Sites between Port-Cartier and the west of the BSI; Zone 2 = Sites inside the BSI; Zone 3 = Sites between the east of the BSI and Matamec; IP = Industrial-port zone)

Site number	Zone	Land use	Mean maximum depth (m)
1	1	Forest	11.5
2	1	Forest	12.2
3	1	Urban	13.2
4	1	Urban	11.7
5	1	IP zone	15.3
6	1	IP zone	16
7	1	IP zone	16.3
8	1	IP zone	10.2
9	1	Forest/IP zone	25.5
10	1	Residential	8
11	1	Brochu River	5.7
12	1	Beach-Residential	19.3
13	1	Ste-Marguerite River	21.3
14	1	Beach/Forest	19.2
15	1	Beach/Forest	19.8
16	2	IP zone	19.8
17	2	IP zone/Anse à Brochu	3.3
18	2	IP zone/Anse à Brochu	7.8
19	2	IP zone/Anse à Brochu	20.2
20	2	IP zone	14.8
21	2	Ship mooring zone	13
22	2	Ship mooring zone	14.2
23	2	Ship mooring zone	16.7
24	2	Urban	9.8
25	2	Urban	3
26	2	Urban-IP zone	23.2
27	2	IP zone	30.5
28	3	Beach/Forest	15
29	3	Beach/Forest	14.3
30	3	Moisie River	28.7
31	3	Moisie River	48.3
32	3	Beach/Forest	16.2
33	3	Matamec River	15.2
34	3	Ecological reserve	15
35	3	Ecological reserve	24.8

environmental variables were explored. Scatter plots with LOESS curves to observe general trends were generated and Spearman correlation was used to assess the significance of these relationships. [A summary of the variables measured in the surface water of the three site zones for each month of sampling is available in the annex \(Table A2\).](#)

145 2.2 **Determination of the thermocline** Water column structure and light attenuation

Thermocline layers were identified, if possible, monthly at every site. Determining the depths of the thermocline is not always straightforward, as several methods can be used (de Boyer Montégut et al., 2004). These methods are however rarely

applied in areas as shallow as in this study. Janecki et al. (2022) found no studies of this sort except in the Baltic Sea, where depths still reached 100 m (Leppäranta and Myrberg, 2009). These authors developed a new algorithm for shallow seas to find the top of the thermocline and halocline, for sites reaching >100 m. We decided for this study to use the gradient threshold method of 0.2 °C (de Boyer Montégut et al., 2004; Leppäranta and Myrberg, 2009). We assumed that the top layer of the thermocline was located at the depth of the strongest gradient of the slope ($\Delta T > 0.2$ °C), and the lower layer was located at the depth of the deepest gradient, to capture the typical plateau, if there was one. Since the sites in our study area were shallow, between 4 and 52 m with an 18 m median, we decided to start the calculations at 3 m depth instead of the advised near-surface 10 m depth (de Boyer Montégut et al., 2004). This approach also avoided the possible effects of the instrument, the anchor and the boat, which can mix the surface waters (de Boyer Montégut et al., 2004; Maske et al., 2014). The depths of the thermocline layer were obtained with the package “rLakeAnalyzer” (Winslow et al., 2019), with some modifications of the “therm.depth” function. A cutoff of 1 °C was also applied, a default criterion in the R function. If the change between surface and maximum depth temperatures was less than this threshold, thermocline depth was not calculated. Thermocline depths were not calculated for sites with a maximum depth < 5 m. [The same gradient threshold method was applied to salinity and density profiles to identify the halocline and pycnocline.](#) We chose to use temperature [in the present study to define the layers as an indicator of vertical stratification](#) since some measurements of salinity were not recorded by the CTD. [Additionally, recent studies have focused on the thermocline in similar environments with dynamic coastal waters influenced by water masses and anthropogenic activities \(Lim et al., 2025\). The euphotic depth was also calculated using the depth at which PAR declined to 1% of the surface value \(Kirk, 1994\), and the stratification index as the density difference between the deepest and the surface \(3m\) sampled depth levels \(Blais et al., 2019\). The diffuse attenuation coefficient \$K_d\$ \(PAR\) \(\$m^{-1}\$ \) was calculated for each CTD profile using linear regression of the natural log of PAR against depth, following Lund-Hansen \(2004\). Profiles with a maximum depth < 5 m, or \$r^2 < 0.8\$ were excluded. Simple and multiple linear regressions were then performed between \$K_d\$ and depth-averaged in vivo fluorescence and turbidity to examine the drivers of light attenuation. One site out of the 35 was chosen to present-illustrate seasonal changes in the vertical profiles of temperature, salinity, Chl *a* and PAR in detail during the sampling season.](#)

3 Results

3.1 Temperature and thermocline

|| 75 In May, [the water](#) temperature was the coldest and was mostly even across depth at all sites (Fig. 2). Surface temperature

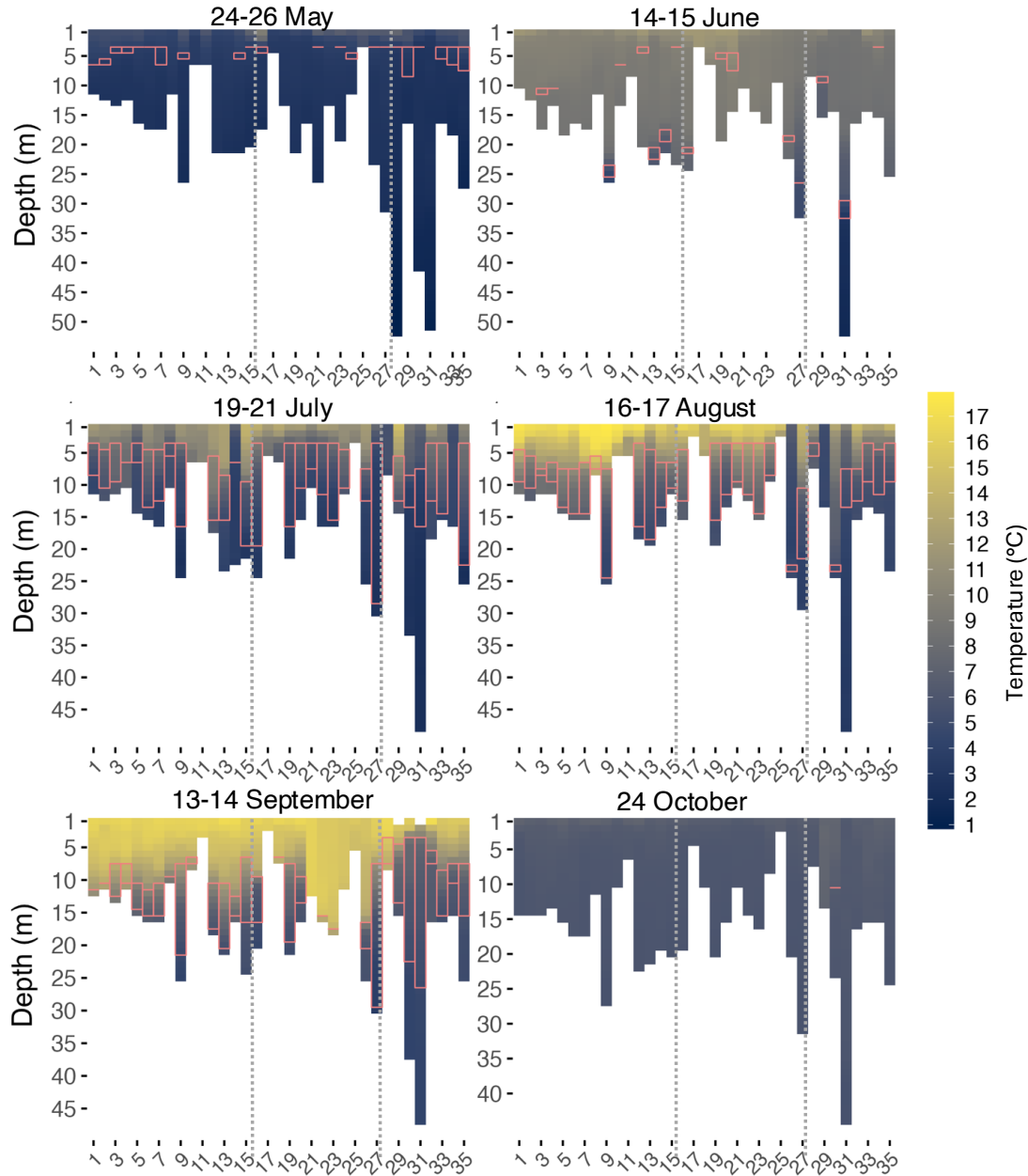


Figure 2: Temperature heatmaps for every month at every site (x axis) along the transect. Dotted lines indicate division of Zones 1 (West), 2 (BSI), and 3 (East), from left to right. The pink rectangles represent the thickness of the thermocline layer.

180 averaged 5.56 °C along the transect. At maximum depth, temperatures ranged between 0.85 °C (Site 31) and 3.83 °C (Site 11), excluding site 25 which was only 3 meters deep. During this period, a near-surface thermocline was beginning to form (Figs. 2 and 3), usually between 3- and 4- m depth (Table A3). In May, 22 sites showed the onset of stratification. In June, surface temperatures began to rise, ranging from 8.69 °C (site 32) to 11.99 °C (site 19). The water column remained largely

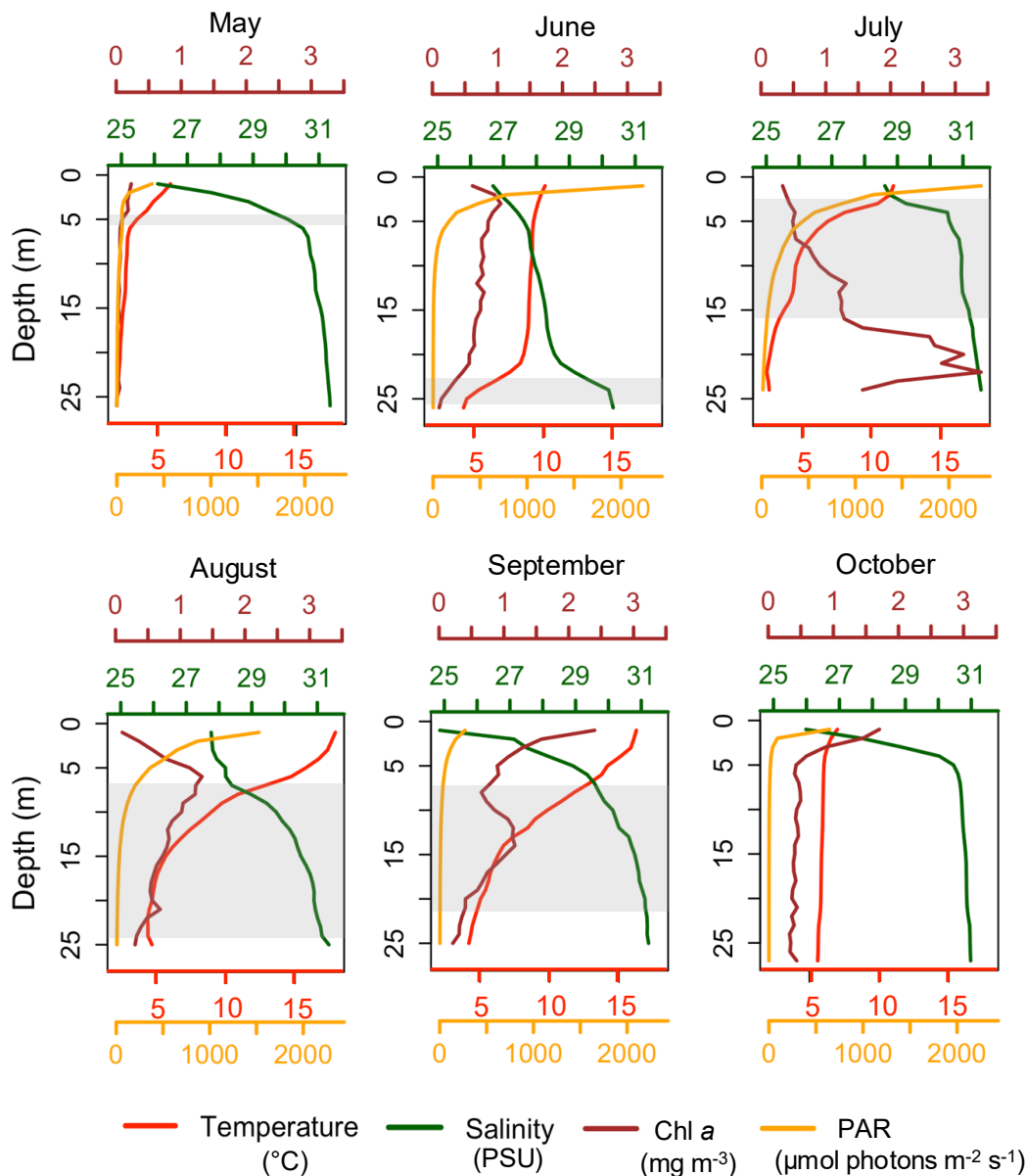


Figure 3: Vertical profiles of temperature, salinity, Chl *a* and PAR at Site 9, on each sampling date. The gray box represents the thermocline layer.

185 mixed, but stratification became noticeable at deeper sites, such as sites 9, 27 and 31, where temperatures were between
1.72 °C (Site 31) and 4.3 °C (Site 9) at maximum depth. Sixteen sites exhibited thin thermocline layers (1-2 m thick),
mostly near the bottom of the water column. Waters in June were generally well-mixed.

190 Between July and September, clear stratification developed with increasing temperatures, though a few shallow sites, < 6
meters depth, lacked distinct layers. At most sites in July, a thermocline was observed between 4 m and 5 m depth. Surface
temperatures ranged from 5.52 °C (Site 28) to 14.80 °C (Site 29). While surface warming was observed at some sites, 14
sites recorded a colder surface temperature than in June. For instance, recorded temperature at site 34 was 10.15 °C in June
versus 5.63 °C in July. Temperature became colder at shallower depths in July, contrasting with June's well mixed
conditions where colder waters only appeared at the deepest sites. In August, surface temperatures ranged between 5.18 °C
195 (Site 29) and 17.92 °C (Site 9). Stratification was still persistent but started to deepen. August showed a deepening of the
thermocline: up to 4 m at some sites (5 and 6) in the west, while sites in the BSI, like sites 19 to 24, showed the same depth
layers as in June. At the eastern sites, the thermocline deepened between 4 and 12 meters. September marked the warmest
month throughout the water column, although deeper sites like sites 31, 30 and 9 retained colder bottom temperatures,
around 4.2 °C. At several western sites, the thermoclines continued to deepen, while they began to disappear at the BSI sites
200 and became shallower toward the east, near the Moisie River (sites 30 and 31). By October, the entire transect showed
uniform temperatures with no significant differences between surface and maximum depths, and the absence of a
thermocline. In early fall, the overall mean surface temperature was 6.83 °C, with 5.55 °C at maximum depth, resulting in an
average difference of only 1.28°C throughout the water column. All sites were mixed, except for site 31, the deepest one,
that showed a weak persistent thermocline at around 10 meters depth. [The stratification index confirmed this trend, with
205 mean values peaking in August and September \(2.9 km/m³\) and dropping in October \(0.7 km/m³\) across all zones \(Table
A3\).](#)

In summary, surface temperatures increased from May to September, with stratification becoming prominent in July. By
October, conditions in the transect had reversed back to cold, uniform temperatures across depths. The largest changes in
210 surface temperatures occurred between May and June (increase of 5.02 °C), and September and October (a decrease of 9.30
°C). Site 9 was chosen as an example (Fig. 3) to show how the thermocline layer, using the threshold method, matched with
the vertical profiles of temperature and other parameters. This site was approximately 25 meters deep and ~~did not have any~~
~~NA (not available)~~ had no missing values, ~~which made making the~~ visualization easier. At this specific site, the thermocline,
as observed in general, started to appear in May at a shallow depth, deepened during summer and disappeared in October.

Signals of freshwater input at sites near river mouths were apparent in May (Fig. 4), particularly at sites 29 (17.8 PSU), 31

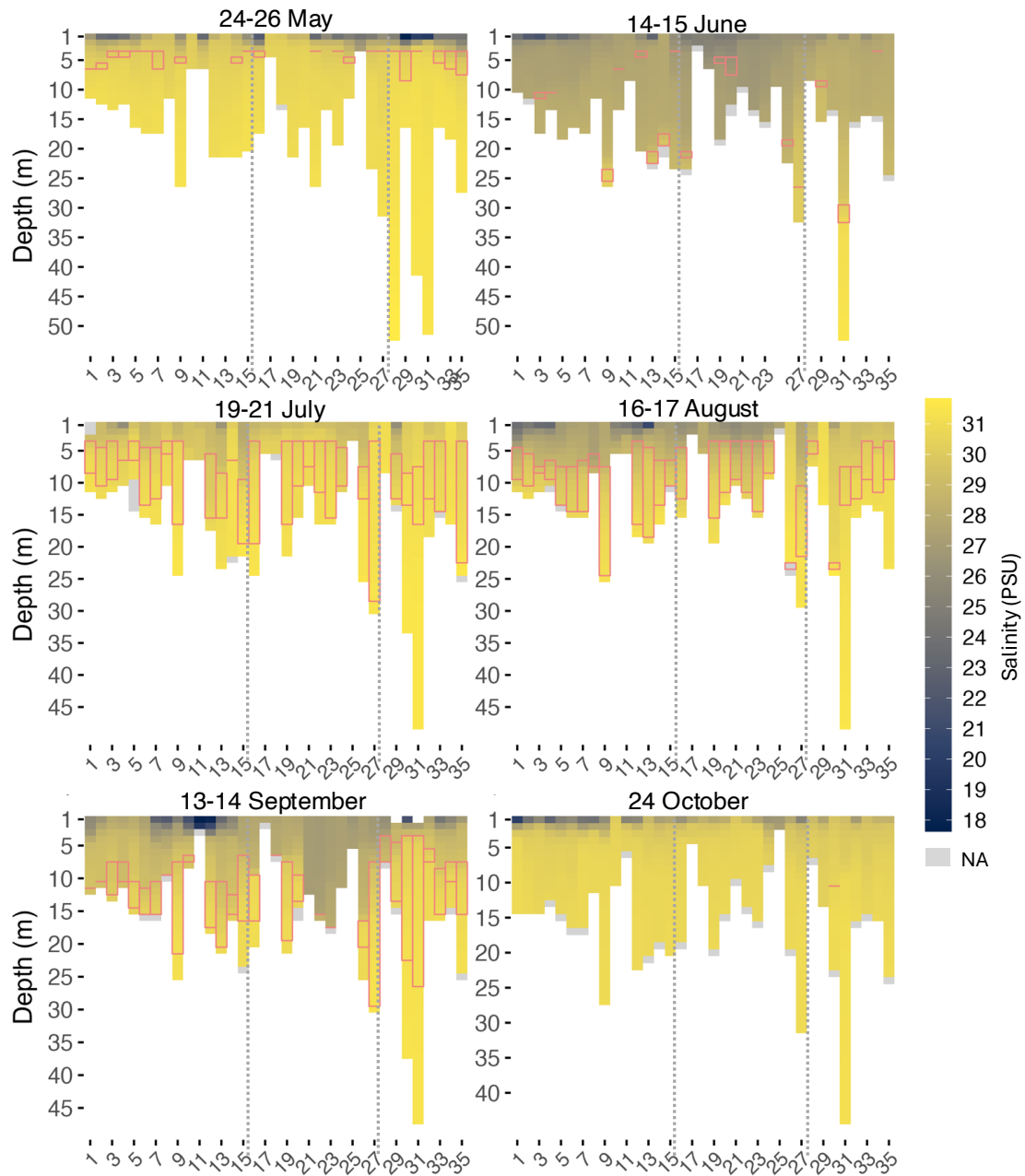


Figure 4: Salinity heatmaps for every month at every site (x axis) along the transect. Dotted lines indicate division of Zones 1 (West), 2 (BSI), and 3 (East), from left to right. The pink rectangles represent the thickness of the thermocline layer.

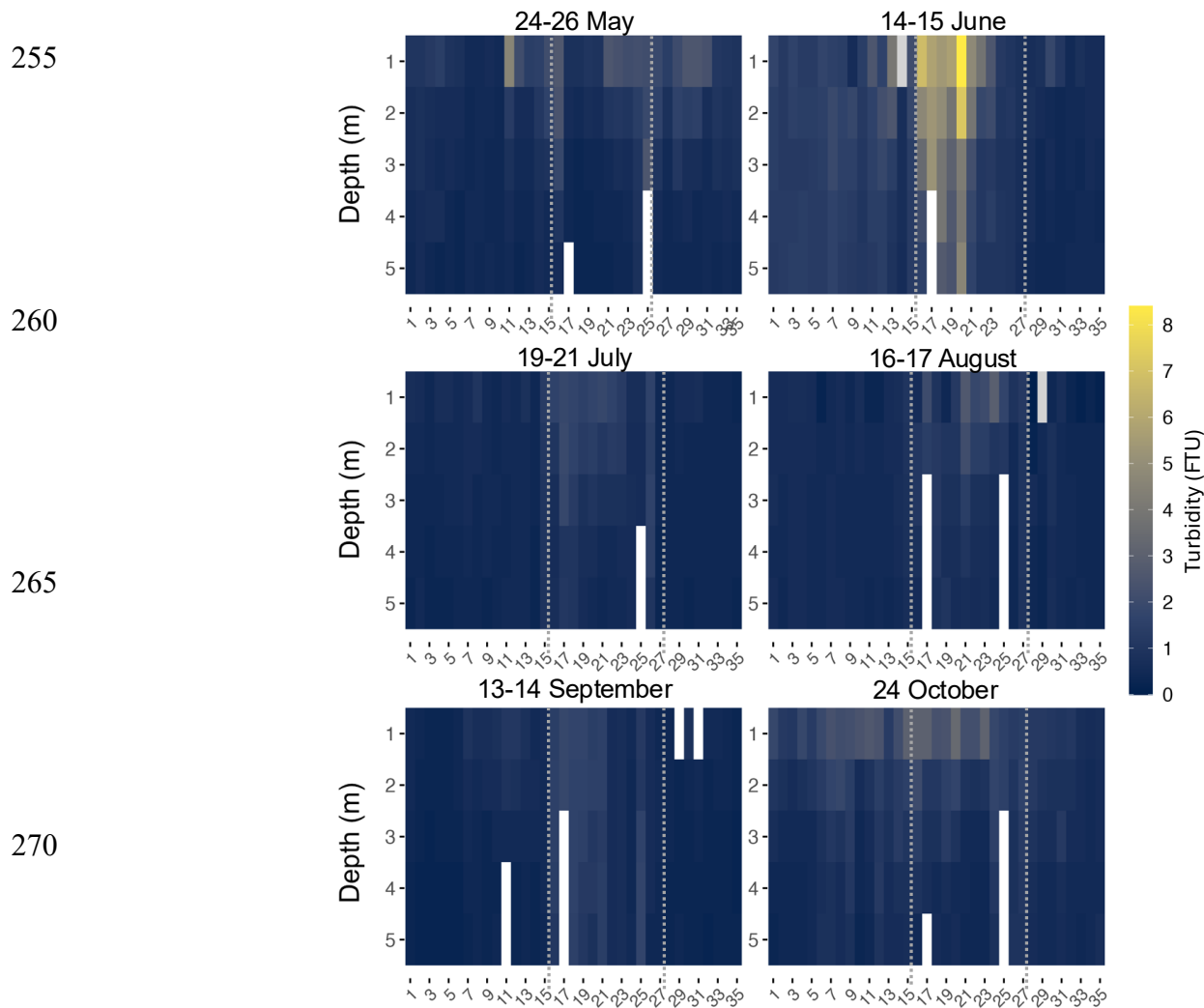
(19.7 PSU) and 30 (20.1 PSU), located near Moisie River. These sites recorded the lowest surface salinity, likely due to increased volume of river discharge following spring snowmelt. The overall average salinity of the water column in May was 30.0 PSU. June recorded an average of 27.8 PSU, the lowest salinity of the season. In contrast, July showed the highest with an average salinity across sites around 30.6 PSU. Stratification became more visible at some sites in July where salinity was lower above the thermocline, such as sites 13 and 15, that recorded 28 PSU versus 30 PSU below. In August, salinity above the thermocline decreased to around 27 PSU, showing the deepening of stratification. A strong signal of freshwater input by rivers was again observed in September, this time near the Brochu and Ste-Marguerite rivers, at sites 11 (17.6 PSU) and 12 (19.1 PSU). In October, salinity was more uniform below the surface, while surface salinity remained lower, especially at sites located west of the transect, where salinity at Site 1 reached 20 PSU at the surface. Below surface, salinity increased to over 30 PSU along the water column.

In these data, salinity inversely followed temperature trends in the water column, where it increased with depth while temperature decreased. This relationship was visible in vertical profiles such as Site 9 (Fig. 3). A Spearman correlation analysis confirmed that temperature and salinity were inversely correlated across the dataset ($r = -0.84$, $p\text{-value} < 0.01$). Overall, salinity at maximum depth showed little seasonal variation, averaging over 30 PSU, except in June (28.5 PSU). The most pronounced seasonal differences in salinity were observed at surface. May and June had the lowest surface salinities whereas July had the highest salinity, and August only showed a slight decrease, in general. A drop in surface salinity was observed in September, especially at sites near the Brochu River (Site 11). Salinity exhibited variability at the surface (first 2 meters), usually at sites located near rivers, and became uniform at depth.

3.3 Turbidity

Because turbidity mostly varied at surface, only data down to a depth of 5 meters was shown for better clarity (Fig. 5). Turbidity across the transect varied between 0 and 8.4 [Formazin Turbidity Units \(FTU\)](#) with limited variability, except at certain sites mostly located inside the BSI (sites 16 to 21). These sites showed a turbidity range of 4.8 to 8.4 FTU, with the highest value measured at site 20.

Higher values of turbidity, superior to 2 FTU, were also recorded in May, in the BSI and at sites near river mouths, such as sites 11 (4.6 FTU), 30 and 31. A similar pattern was observed in October, with higher turbidity values in the BSI and at sites close to rivers, where Site 20 exhibited a surface turbidity of 3.2 FTU and Site 11 a turbidity of 2.6 FTU. In July and September, turbidity remained below 2 FTU throughout the transect, with sites within the BSI being slightly more turbid than the others.



275 **Figure 5: Turbidity heatmaps for every month at every site (x axis) along the transect. Dotted lines indicate division of zones 1 (West), 2 (BSI), and 3 (East), from left to right. The pink rectangles represent the thickness of the thermocline layer.**

3.4 Fluorescence (Chl *a*) and-PAR

A seasonal variation of fluorescence (Fig. 6), reflecting concentration of Chl *a*, was observed along the transect. Concentrations were the lowest in May and began to rise in June, reaching a peak in July, and then decreased throughout August to October. In September, a localized resurgence was observed at the surface of some sites, before fluorescence levels declined again in October at most sites.

280

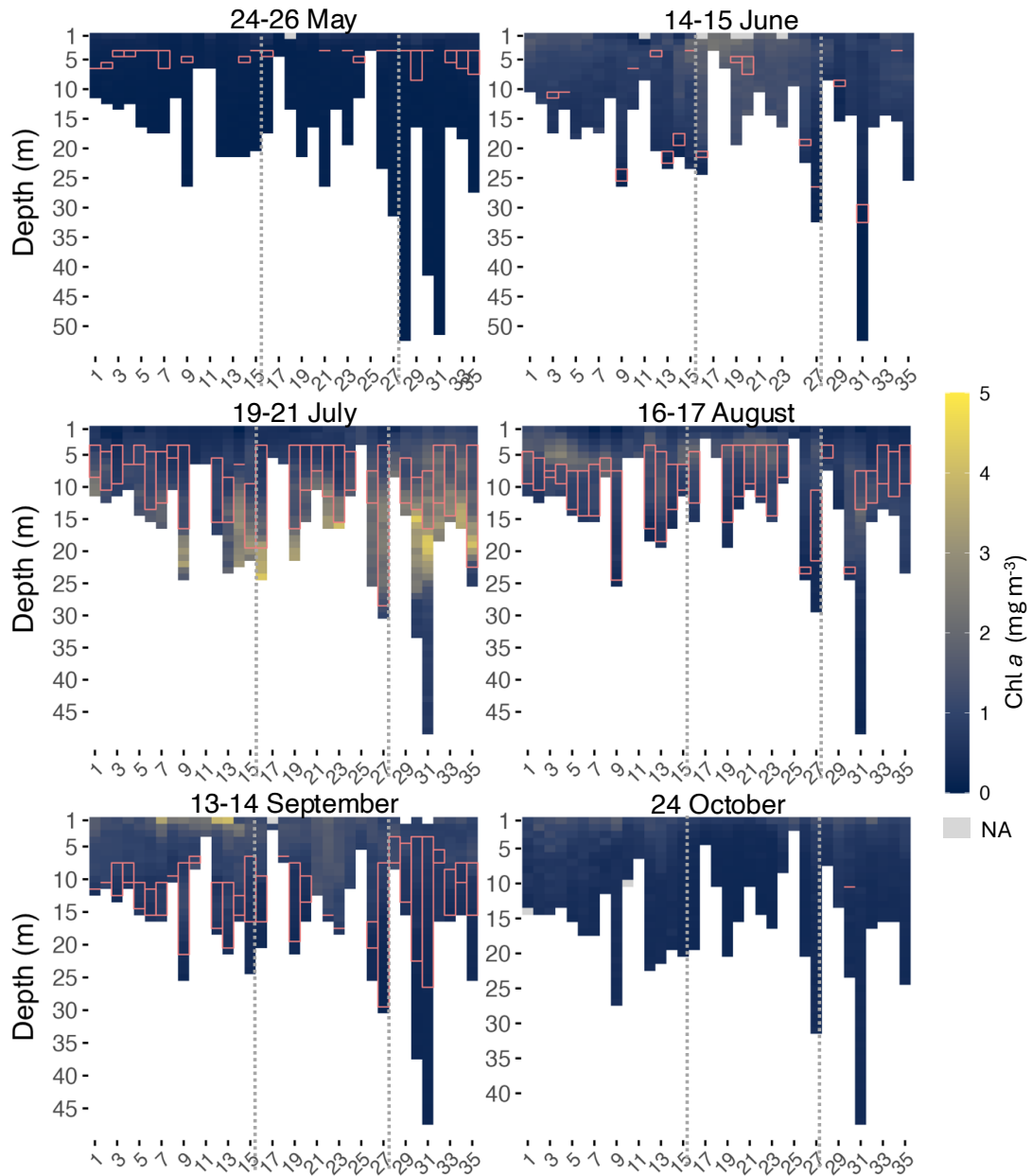


Figure 6: Chl *a* heatmaps for every month at every site (x axis) along the transect. Dotted lines indicate division of zones 1 (West), 2 (BSI), and 3 (East), from left to right. The pink rectangles represent the thickness of the thermocline layer.

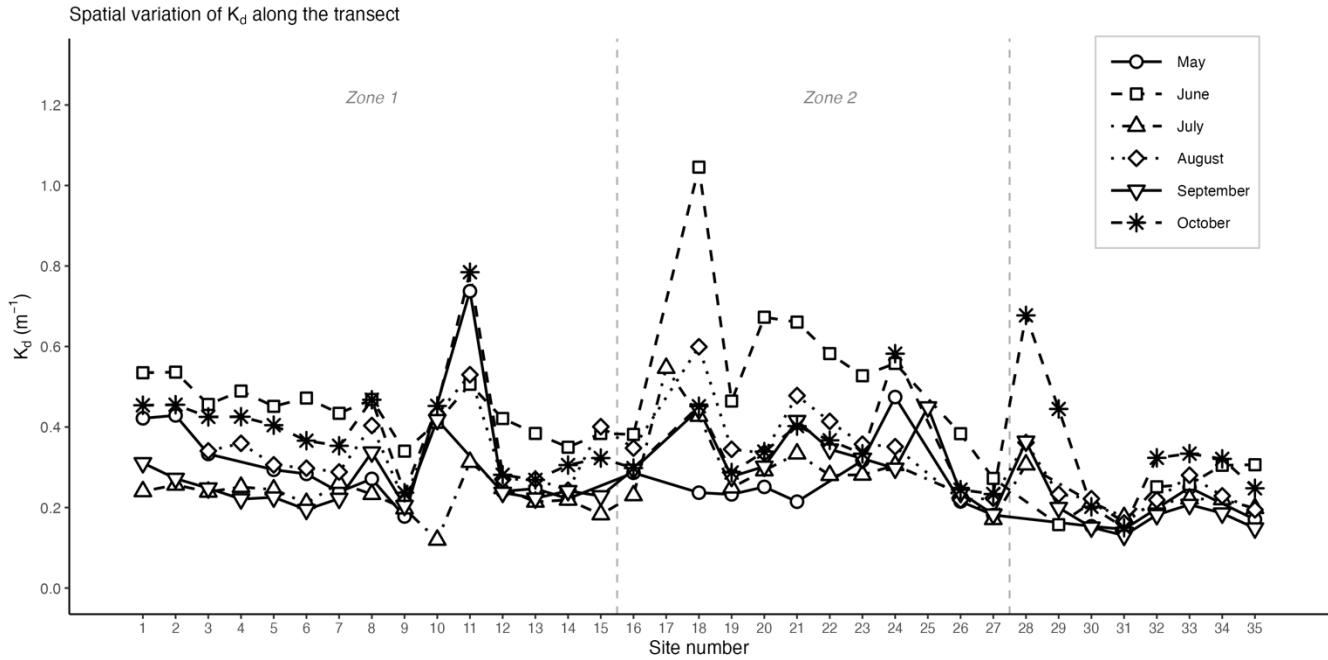
285 In May, [surface](#) fluorescence throughout the transect averaged [0.0970.37](#) mg m⁻³ and [surface](#) PAR [85.5943.8](#) μmol photons m⁻² s⁻¹. All sites had a concentration below 1 mg m⁻³ at all depths. In June, [surface fluorescence increased to a mean of 1.07 mg m⁻³, with surface PAR averaging 1,517.5 μmol photons m⁻² s⁻¹.](#) Sites 17, 18 and 19 recorded the highest Chl *a* concentration. These were the only sites across the entire transect where fluorescence exceeded 2 mg m⁻³ in June, all

290 between 1 and 3 meters. In July, a subsurface fluorescence maximum was observed at several sites, with the highest concentrations ~~were~~ found at sites 30, 31, 16, and 35, followed by Site 23, where concentrations were all superior to 4 mg m^{-3} , at depths between 15 to 24 meters. All these sites were located near rivers, except for Site 16 which was positioned in front of an aluminum smelter. At this site, the highest concentration of 4.28 mg m^{-3} was measured at 24 meters, which was the maximum depth at this site. All fluorescence peaks were below the thermocline layer, except at Site 35 where fluorescence concentrations were higher at the thermocline. Surface fluorescence averaged 0.53 mg m^{-3} in July, while surface PAR averaged $746.1 \text{ } \mu\text{mol photons m}^{-2} \text{ s}^{-1}$, lower than in June. Average PAR in June ($144 \text{ } \mu\text{mol photons m}^{-2} \text{ s}^{-1}$) and July ($145 \text{ } \mu\text{mol photons m}^{-2} \text{ s}^{-1}$) were similar but higher at the surface in June than in July (1,520 compared to $746 \text{ } \mu\text{mol photons m}^{-2} \text{ s}^{-1}$ in July). August showed the highest surface PAR of the season, averaging $292 \text{ } \mu\text{mol photons m}^{-2} \text{ s}^{-1}$ overall, and $1,707 \text{ } \mu\text{mol photons m}^{-2} \text{ s}^{-1}$ at surface, while surface fluorescence averaged 0.57 mg m^{-3} . started to decline with an overall average of 0.94 mg m^{-3} . Sites 3, 4, 5, and 6, all located in Port-Cartier near the aux Rochers River estuary, and Site 31 at the Moisie River, had a concentration superior to 2 mg m^{-3} . Maximum fluorescence (2.73 mg m^{-3}) was observed at Site 300 4 at a depth of 5 m. Highest fluorescence in August occurred at shallower depths than in July, between 5 and 26 m. In contrast to July, peaks of Chl *a* in August were mostly found at shallower depths, either above or within the thermocline layer.

305 In September, surface fluorescence reached its seasonal peak, averaging 1.59 mg m^{-3} , with surface PAR averaging $326.5 \text{ } \mu\text{mol photons m}^{-2} \text{ s}^{-1}$. Sites 7 (3.49 mg m^{-3}), 12 (3.84 mg m^{-3}) and 13 (4.06 mg m^{-3}) recorded higher fluorescence concentrations than in August, all at the surface. Concentrations higher than 2 mg m^{-3} were observed at 8 sites, all located in the western part of the transect. Fluorescence declined again in October, with a mean surface of 1.11 mg m^{-3} . a average fluorescence of 1.11 mg m^{-3} overall. The maximum fluorescence for this month (1.79 mg m^{-3}) was measured at the surface of Site 32, followed by the surface of Site 9 (1.71 mg m^{-3}). October was also the month with the lowest mean PAR ($35.7 \text{ } \mu\text{mol photons m}^{-2} \text{ s}^{-1}$).

3.5 Diffuse light attenuation coefficient; K_d (PAR)

The diffuse attenuation coefficient, K_d (PAR) ranged from 0.12 to 1.05 m^{-1} , with an overall mean of 0.32 m^{-1} , showing both seasonal and spatial variability along the transect (Fig. 7).



315

Figure 7: Diffuse light attenuation coefficient K_d at each site along the transect for the six sampling months. Dashed vertical lines delimit the three site zones.

June had the highest mean K_d (0.43 m^{-1}), where sites 18, 20, 21 and 22 reached values between 0.58 and 1.05 m^{-1} , the highest value recorded along the transect. October showed the second highest mean (0.37 m^{-1}), particularly at sites influenced by rivers such as Site 11 (0.78 m^{-1}) and Site 28 (0.68 m^{-1}), where higher turbidity was observed that month. July had the lowest mean K_d (0.24 m^{-1}), indicating clearer water conditions during the summer stratified period. Throughout all months, the eastern sites showed the lowest K_d values (0.24 m^{-1}), while the BSI had the highest (0.35 m^{-1}).

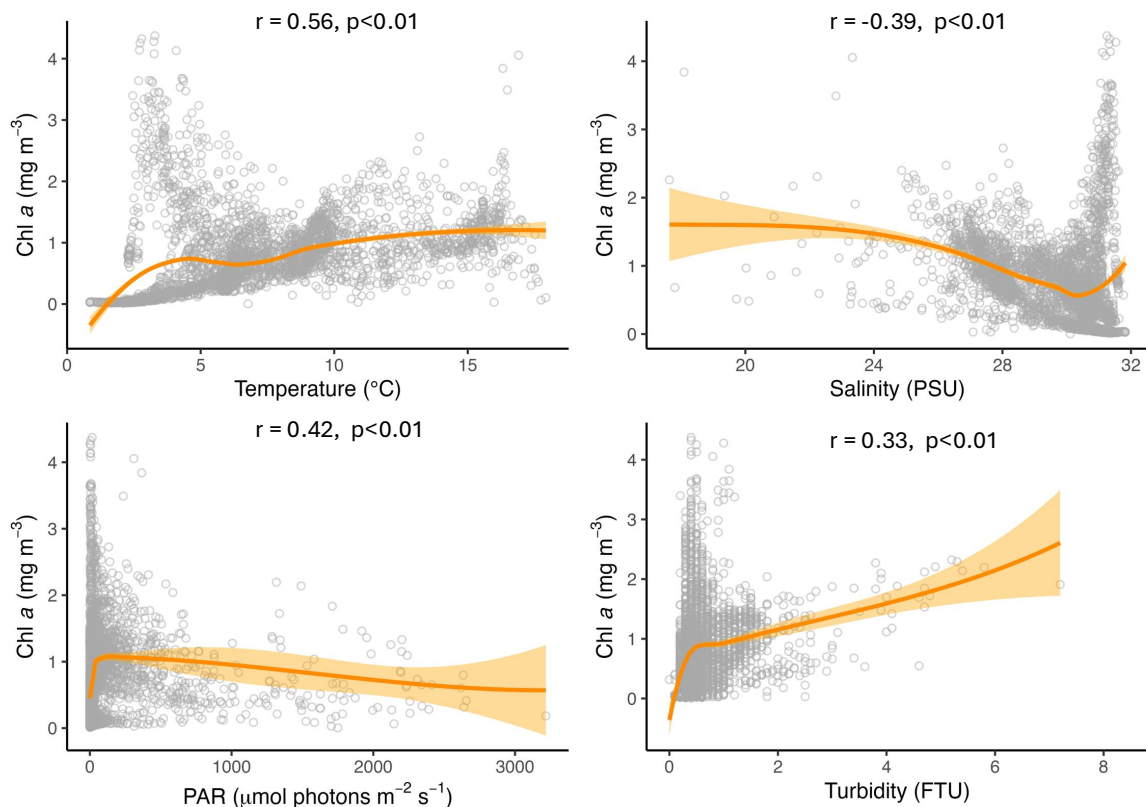
320

A significant positive correlation was found between K_d and depth-averaged turbidity ($r^2 = 0.59$, $p < 0.001$), while the relationship between K_d and depth-averaged fluorescence was weak ($r^2 = 0.02$, $p < 0.05$). Fluorescence was not a significant driver when included alongside turbidity in the multiple regression ($p > 0.05$), suggesting that turbidity, rather than phytoplankton biomass, was the dominant driver of light attenuation, consistent with the elevated turbidity values observed at BSI and river-influenced sites.

325

3.65 Relationship between Chl *a* and environmental variables (temperature, salinity, PAR and turbidity)

330 In this data set, temperature, salinity, turbidity and PAR all had significant effects on Chl *a*, and the scatterplots and LOESS
smoothers revealed nonlinear relationships (Figs. 8 and A1-A47). The highest Chl *a* concentrations were mostly observed at
colder temperatures, particularly between 1 and 5 °C, and at higher salinities between 30 and 32 PSU. However, the monthly
breakdown revealed that the direction of these relationships changed across the season. In May and June, Chl *a* increased
with temperature ($r = 0.89$ and 0.81), while in July the relationship reversed ($r = -0.61$), reflecting the subsurface
335 fluorescence maximum where the highest concentrations occurred at deeper cold temperatures (Fig. A1). Concentrations
then decreased with increasing temperature, with a secondary rise at warmer values, as suggested by the trend. This could
reflect the fewer peaks of Chl *a* near the surface observed in autumn. A negative relationship between Chl *a* and salinity was
observed in most months, suggesting that higher concentrations tended to occur at lower salinities, possibly linked to
localized riverine inflow and associated nutrient inputs. July was an exception, where a positive relationship was observed,
340 likely reflecting the subsurface fluorescence maximum (Fig. A2). ~~A few additional peaks were detected at lower salinities
(<24 PSU), likely indicating the influence of localized riverine inflow and associated nutrients inputs.~~ Peaks of fluorescence
were most abundant under low to moderate light conditions, ~~between 0 and $100 \mu\text{mol photons m}^{-2} \text{s}^{-1}$.~~ When focusing on
Chl *a* peaks only ($>2 \text{ mg m}^{-3}$), the relationship with PAR showed a weak negative correlation ($r = -0.46$, $p < 0.01$) as opposed
to a weak positive one with all the data ($r = 0.42$, Fig. 87), consistent with the subsurface fluorescence maximum observed in
345 July (Fig. A3). These peaks mostly occurred between 0.88 and $1,491 \mu\text{mol photons m}^{-2} \text{s}^{-1}$, with a median of $16.9 \mu\text{mol}$
 $\text{photons m}^{-2} \text{s}^{-1}$. This was also visible at Site 9 (Fig. 3), where in July, peaks ($>3 \text{ mg m}^{-3}$) were below the thermocline at low
PAR between 19.8 and $29.2 \mu\text{mol photons m}^{-2} \text{s}^{-1}$. Turbidity measurements were mostly between 0 and 2 FTU during the
sampling period, which coincided with most of the Chl *a* peaks and was positively associated with Chl *a* in most months
(Fig. A4). ~~Given the nonlinear nature of the relationships, Overall, the strength and direction of the relationships between
350 Chl *a* and the environmental variables varied across months, highlighting the seasonal dynamics along the transect.
Spearman correlations only revealed moderate positive associations for all variables, except for salinity, which exhibited a
negative trend.~~



β55 **Figure 87:** Scatter plots showing the relationships between Chl *a* and temperature, salinity, PAR and turbidity across the transect. The orange line represents the LOESS curve with 95% confidence interval (shaded area). The Spearman correlation (*r*) and its *p*-value are also indicated.

4 Discussion

This study shows that the water column properties near the coast of the Sept-Îles area undergo changes during the ice-free season, shifting from cold, well-mixed waters in spring to pronounced stratification in summer, particularly in July and August. The thermal stratification gradually deepens in September and disappears by October, with waters mixing and returning to more uniform conditions in autumn. Our study also highlights seasonal variability in Chl *a*, with high concentrations observed below the thermocline in July and fewer peaks observed at the surface in September near river sites. Most of the Chl *a* peaks recorded through the season, occurred in July, at lower temperatures and higher salinity ~~observed in~~ July. Based on this dataset gathered in 2022, the Sept-Îles area shows the typical seasonal variability of a temperate coastal environment (Cloern, 1991; Leppäranta and Myrberg, 2009; Galbraith et al. 2024b; Lim et al., 2025). In the Gulf of St. Lawrence, phytoplankton blooms are generally observed in spring followed by a secondary bloom in autumn (Galbraith et al., 2024b). However, this pattern differs in the present study, since the main bloom was observed during summer, perhaps due to the fact that we did not sample at the end of April, when the spring bloom might have occurred. Previous studies on

370 pigments and phytoplankton assemblages carried out in the BSI, reported similar results; a seasonal variability in primary
production with peaks of Chl *a* occurring in April, June and September (Lefebvre, 2023; Araújo et al., 2022). This seasonal
dynamic may already be influenced by current climate change. The Gulf of St. Lawrence, historically covered with sea_ice
until mid-March, has experienced 4 nearly ice-free winters since 2010 (Galbraith et al., 2024a). Changes in sea_ice cover are
also occurring in the BSI, where sea_ice has been disappearing sooner than usual over the past few years, and its formation
375 and movements are becoming unpredictable (Allard, 2025). According to Allard (2024), these changes during the winter
season could impact primary productivity in the BSI. Sea_ice changes can affect spring bloom timing and the composition of
phytoplankton species, thus impacting the whole food web (Pärn et al., 2022; Castagno et al., 2023; Nielsen et al., 2024). A
possible small trend towards an earlier and more intense spring bloom was observed by Laliberté and Larouche (2023)
between 1998 and 2019 in the St. Lawrence Estuary and Gulf, and they associated this trend with the decreasing length of
380 the sea_ice season.

In May, temperature and salinity were stable across the water column, but a warmer_ and brackish surface layer started to
develop, marking the beginning of thermocline formation. This layer is heated by the sun during summer, while freshwater
continues to flow from rivers into the coastal area. As observed in our study, lower salinity was mostly found at localized
385 places in proximity to estuaries+rivers, e.g., sites 29, 30 and 31, near the Moisie River in May and sites 11 and 12 next to the
Brochu and Ste-Marguerite rivers in September, all coinciding with peak river discharge (Carrière et al., 2018a). The influx
of freshwater also increased turbidity at river-influenced sites such as Site 11, next to Brochu River. The well-mixed water
column in May, and June, could also be linked to wind. Wind speeds recorded during these two months were stronger than
those observed in the other months (Table A1). Phytoplankton abundance remained minimal with fluorescence averaging
390 0.097 mg m⁻³. Lefebvre (2023) identified April and May as the most productive months in the BSI during summer 2017, an
observation that does not align with our study, as all concentrations of fluorescence were below 1 mg m⁻³ in May 2022.
According to Araújo et al., (2022) the spring bloom in the BSI in 2017 occurred in April to early May before the spring
freshet, when diatoms were the main phytoplankton group. Our first sampling was conducted at the end of May, between
the 24th and the 26th, probably after the spring bloom. Furthermore, Araújo et al. (2022) and Lefebvre (2023) using the same
395 dataset, carried out their sampling mostly at the surface, whereas we measured the whole water column, which could be
another reason explaining the differences in our results.

In mid-June, the water column was generally warmer, except at deeper sites such as Site 31, which reached 52 m in depth. A
deeper thermocline layer marked the limit between the warmer mixed layer and the colder, saltier deep waters. As for
400 variation in Chl *a*, only a few sites (17, 18 and 19, all located in the BSI in front of Anse à Brochu) recorded a Chl *a*
concentration exceeding 2 mg m⁻³. These sites also recorded the highest turbidity and still showed highest concentrations of
Chl *a* along the transect. Usually, turbidity limits phytoplankton biomass by reducing light penetration (Cloern, 1987; May et
al., 2003). However, given the shallow depth at these sites, particularly sites 17 (2 m) and 18 (6 m), it is possible that the

sampling process, including boat anchoring and the use of the CTD instrument, contributed to sediment resuspension. It
405 could have brought particles from the bottom layer to the surface and affected turbidity measurements. Wind, tides and
waves can also have an influence at these shallow sites. Furthermore, the presence of phytoplankton or other organisms also
affects turbidity measurements. However, such high turbidity levels were only observed in June. Another explanation could
be the location of Anse à Brochu that is at proximity ~~of~~to industrial activities and private docks. This area is also next to a
410 discharge point for stormwater and municipal sewage discharge (Carrière et al., 2018b). Given the importance of these
industries and the traffic of vessels, it is possible that these aspects contributed to sediment resuspension, influencing Chl *a*
concentration. This also aligns with Lefebvre (2023), who observed a peak of Chl *a* ($> 5 \text{ mg m}^{-3}$) at this same location in
June 2017, associated with a dinoflagellate bloom. Furthermore, Liu et al. (2018), found that in high turbidity environments,
temperature had a greater impact than light intensity on the timing of blooms. This could potentially be the case in our study.

415 Thermal stratification appears to play an important role in structuring plankton communities. Lim et al. (2025) found that
plankton diversity and richness in coastal waters of southern Korea were lowest in July, coinciding with strong thermocline
formation, whereas diversity peaked in September when stratification weakened. Additionally, their results indicated that
plankton abundances below the thermocline were significantly lower than in the upper layer. In contrast, our study found that
420 the highest Chl *a* concentrations were in July and were predominantly located below the thermocline. As seen in figures 2
and 7, the highest concentration of Chl *a* was deeper in the water column and at low to moderate PAR, but where nutrients
are sufficient for growth. However, nutrients were not measured in the present study. In oceanic environments, Chl *a*
concentration varies dynamically and often shows maximum values in the subsurface of the layer rather than at the surface
(Yasanuka et al., 2022). In the East China Sea, similar results were found, where the highest Chl *a* concentrations were
425 recorded at the bottom of the thermocline. This was associated with a change in nutrient concentrations, where
phytoplankton had access to a greater supply of nutrients at depth (Wu et al., 2002). Given that nutrient availability is a key
driver for phytoplankton in the water column (Browning and Moore, 2023; Wei and Zhao, 2025), the higher Chl *a*
concentrations below the thermocline in our study could potentially be explained by nutrient accumulation in deeper layers
rather than light availability. However, some studies still find high Chl *a* concentrations even when nutrients are depleted, as
430 observed in the Baltic Sea (Stramska and Jakacki, 2024). This suggests that other processes, such as upwelling events and
currents, may also influence Chl *a* distribution. For example, at some locations of our transect, environmental conditions
changed in July compared to June. Site 34, for example, recorded a decline in temperature from 10.2 °C to 5.63 °C during
this time. Likewise, Site 31 (near ~~the~~ Moisie River) exhibited higher salinity in July than in June. Furthermore, most peaks of
Chl *a* occurred at lower temperatures and high salinity (Fig. 7), suggesting potential upwelling events. Several areas in the
435 Gulf of St. Lawrence, including the north shore of the Gulf, are known to be in upwelling areas (Bourque and Kelley, 1995;
Doyon and Ingram, 2000). These events are often associated with high Chl *a* concentrations, as they bring cold, nutrient-rich
deep waters to the surface (Roegner et al., 2011; Diez-Minguito and de Swart, 2020). A 22-year time series by Laliberté and
Lerouche (2023) showed a strong positive trend in Chl *a* along the Gulf's North Shore, that they associated with stronger

upwelling events generated by favorable winds. Modeling studies suggested that increased wind speeds may enhance upwellings along the north coast of the Gulf, potentially offsetting surface warming (Long et al., 2016). Although no long-term data currently exists for our specific study area, the elevated wind speeds observed in July may have facilitated vertical mixing and nutrient transport, contributing to the observed Chl *a* maxima. [The vertical concentration of Chl *a* below the thermocline in July may also partly explain why fluorescence was a weak predictor of light attenuation compared to turbidity along the transect. Since *K_d* integrates attenuation throughout the entire water column, Chl *a* peaks that are lower in the water column, would contribute less to overall light attenuation than particles from the surface. Unlike findings in some estuarine environments where phytoplankton and suspended particulate matter both contributed to light attenuation \(Lund-Hansen, 2004\), turbidity was the dominant driver in the Sept-Îles area. This suggests that inputs from rivers and activities in the BSI played a greater role than phytoplankton biomass in controlling light availability. This is consistent with the higher light attenuation observed at river-influenced and urban sites, particularly within the BSI, compared to the eastern sites which showed lower attenuation reflecting a more pristine environment.](#)

By August, we observed that the highest Chl *a* concentrations ($>2 \text{ mg m}^{-3}$) had shifted above the thermocline. This shift may have been driven by surface heating, with observed temperatures increasing during summer between July and September. This deepens the thermocline over time and alters vertical distribution patterns, contributing to variability in phytoplankton abundance. The surface layer in August also showed a lower salinity above the thermocline, reflecting river runoff and the beginning of the secondary summer bloom observed here and in earlier studies (Carrière et al., 2018a; Lefebvre, 2023).

September brought the warmest water temperatures of the year, likely due to heat accumulation over the summer months. Air temperature reached its peak between mid-July and mid-August (Table A1), contributing to the deepening of the thermocline during this period. Despite differences between our spring results and those of Araújo et al. (2022) and Lefebvre (2023) in the BSI, we found similar results for September. Fluorescence showed surface peaks at sites 7, 12 and 13, located outside the BSI. Although these peaks were at different locations than those sampled by Lefebvre (2023), who focused on sites within the BSI, they still demonstrate that there is observable phytoplankton activity in early autumn. The location of these peaks also suggests environmental [and anthropic](#) influences. Site 7 is in proximity to the industrial zone of Port-Cartier, close to the outflow of several streams, and sites 12 and 13 are located near the Brochu River. The latter is of ecological significance as a highly productive salt marsh ecosystem is found at its mouth (Bourque and Malouin, 2009). These sites also exhibited freshwater influence since they represented the area along the transect with the lowest surface salinity, especially in September. However, turbidity at these sites remained relatively low, averaging only 1 FTU. This could indicate a peak in river discharge influencing phytoplankton dynamics through nutrient inputs, that were not measured for this study. A study in a similar environment, a Chinese bay under anthropogenic effects, found that nutrients via river inputs had the greatest influence on Chl *a* concentrations (Wang et al., 2024).

Finally, the water column returned to well-mixed conditions in October, with fluorescence declining, and the complete disappearance of the thermocline, with the exception of Site 30 that still showed a residual deep thermocline. In the first meter at surface along the transect, freshwater influence was still noticeable but did not impact the rest of the water column. 475 October recorded higher turbidity at certain sites, mostly located within the BSI. The BSI has a counterclockwise circulation, which tends to concentrate freshwater discharges from the four rivers in the Pointe-Noire area (Shaw et al., 2022; Paquette et al., 2018). This circulation pattern likely explains the elevated turbidity in this area in October, while also accounting for the absence of a freshwater signal despite the numerous streams and rivers flowing into the BSI.

5 Data availability

480 The complete CTD data used in this study are available in the Borealis database: <https://doi.org/10.5683/SP3/ALRWON> (Arseneault & Saulnier-Talbot, 2025a).

6 Conclusion

This study of water column dynamics during the ice-free season in a subarctic coastal environment documented seasonal variability of key ecological parameters including temperature, salinity and Chl *a*. The region of Sept-Îles has a highly 485 dynamic coastal ecosystem where environmental conditions fluctuate daily. Although the typical spring bloom was not recorded, likely due to sampling starting after its peak, seasonal trends in thermocline formation and Chl *a* distribution were observed throughout the ice-free season. This clear seasonal variability has also been observed in similar environments such as the South of the Baltic Sea, where a thermocline forms in the beginning of May and starts to deepen in September due to autumn cooling (Leppäranta & Myrberg, 2009). However, due to the dynamic nature of the study area and its shallow 490 depths, thermoclines and observed water column trends can change within a day. For instance, Carrière et al. (2018a), could not detect a thermocline in the BSI in summer 2016, potentially due to sampling dates that may not have aligned with peak stratification periods. Furthermore, lowest salinity values occurred during spring and early fall, coinciding with peak river discharge. Paquette et al. (2018) explained that these local freshwater layers can persist from a few hours to a few days in calm conditions. The results of our study depict the near-shore water columns at specific dates, as sampling was carried out 495 only once per month. This shows how phytoplankton biomass variability is high in dynamic environments with complex physical parameters interactions, as previously suggested in similar studies (e.g. May et al., 2003).

Incorporating nutrient and oxygen monitoring would be essential to further improve our understanding of the mechanisms driving Chl *a* variability in the water column of this region and detecting potential upwelling events or eutrophication. Sept- 500 Îles represents a high-use coastal ecosystem, under the influence of climatic and anthropogenic pressures, highlighting the importance of long-term and regular monitoring to detect environmental changes. Climate-related impacts such as changes in

sea-ice cover, wind regimes and the intensity of upwelling events may influence primary productivity. Therefore, regular monitoring of the water column, especially Chl *a*, is crucial to detect trends in phytoplankton dynamics and to assess broader ecological impacts of environmental change. This study complements prior work and will be useful for future studies and environmental monitoring in the region.

Appendices

Table A1: Meteorological data for sampling days (in bold) and the previous week. Data retrieved from the Government of Canada at the Sept-Îles Station (Government of Canada, 2025). Temperatures are air temperature (no water temperature data is available).

Dates	Max temp. (°C)	Min temp. (°C)	Mean temp. (°C)	Total precipitation (mm)	Max speed gust (km/h)
17/05/2022	5.9	4	4.9	31.7	58
18/05/2022	9.3	-1.8	3.8	2.9	53
19/05/2022	13.6	-2.5	5.6	0	<30
20/05/2022	14.1	3.7	8.9	0.3	<30
21/05/2022	8.7	7	7.9	6.1	31
22/05/2022	15.3	6	10.7	11.6	32
23/05/2022	13.7	-2.4	5.7	0	39
24/05/2022	15.4	-2.8	6.3	0.3	<30
25/05/2022	19.3	0.6	9.9	0.6	39
26/05/2022	11.8	4.7	8.2	7.1	38
07/06/2022	17	5.6	11.3	0	35
08/06/2022	14	9.3	11.6	14.3	54
09/06/2022	11.6	9.1	10.3	11	45
10/06/2022	12.3	9.2	10.8	18.2	44
11/06/2022	19.9	9.3	14.6	4	<30
12/06/2022	17.7	5.8	11.7	0	<30
13/06/2022	17.2	10.8	14	0.8	54
14/06/2022	18.8	10.3	14.6	0.2	<30
15/06/2022	23.4	8.6	16	0	<30
12/07/2022	17.5	13	15.3	25.7	<30
13/07/2022	22	6	14	0.2	42
14/07/2022	19.8	6.2	13	0	<30
15/07/2022	25.4	10.4	17.9	0	36
16/07/2022	19.5	10.9	15.2	0	<30

17/07/2022	22.6	10.4	16.5	0	<30
18/07/2022	21.5	13.9	17.7	0.5	<30
19/07/2022	20.7	14.8	17.8	0	41
20/07/2022	26.3	14.5	20.4	0	46
21/07/2022	23.2	12.3	17.7	7.9	36
09/08/2022	19.5	7.5	13.5	0.2	NA
10/08/2022	17.9	5.6	11.8	0.4	NA
11/08/2022	NA	NA	NA	NA	NA
12/08/2022	20.8	11	15.9	0.3	<30
13/08/2022	21.8	9.4	15.6	0.5	<30
14/08/2022	20.6	9.2	14.9	1.8	<30
15/08/2022	22.5	10	16.2	0.5	<30
16/08/2022	25.6	11.3	18.4	0.2	<30
17/08/2022	24	14.1	19	0	<30
06/09/2022	15.7	1.6	8.6	0	<26
07/09/2022	17.2	8.7	12.9	0	<30
08/09/2022	16.1	9.3	12.7	3.9	<30
09/09/2022	15.4	9.8	12.6	0.2	<30
10/09/2022	17.4	12.5	14.9	0	<30
11/09/2022	15.3	10.4	12.8	0	<30
12/09/2022	23	9.1	16	0.3	<30
13/09/2022	17.4	11	14.2	0	<30
14/09/2022	16.5	11.4	13.9	12.5	45
17/10/2022	12.6	2.6	7.6	0.3	<30
18/10/2022	9.4	6.7	8	20.5	63
19/10/2022	10.1	8.4	9.2	49.4	62
20/10/2022	9.1	4.1	6.6	3.6	<30
21/10/2022	8.6	4.7	6.7	0	34
22/10/2022	11.3	-0.3	5.5	0	<30
23/10/2022	16.4	-1.2	7.6	0	<30
24/10/2022	11.7	0.5	6.1	0	<30

510

[Table A2: Mean, standard deviation and range of temperature, salinity, turbidity, fluorescence, and PAR in the surface water of the three site zones for each month of sampling.](#)

Month	Zone	Temperature (°C)			Salinity (psu)			Turbidity (FTU)		
		Mean	SD	Range	Mean	SD	Range	Mean	SD	Range

May	1	5.11	0.79	4.25 – 7.08	26.78	2.35	23.26 – 29.68	1.34	1.04	0.5 – 4.6
	2	5.98	1.54	3.9 – 9.5	26.05	2.65	22.29 – 30.04	1.72	0.69	0.8 – 2.6
	3	5.65	1.01	4.21 – 7.45	22.23	2.92	17.8 – 25.0	1.76	0.73	0.9 – 2.5
June	1	10.77	0.52	10.06 – 11.74	24.96	1.94	21.76 – 27.74	1.71	0.79	0.6 – 4.0
	2	10.9	1	9.43 – 11.99	25.41	0.76	24.53 – 26.43	4.2	2.55	0.8 – 8.4
	3	9.63	0.84	8.69 – 11.22	27	0.73	26.25 – 27.84	0.86	0.42	0.5 – 1.8
July	1	10.9	1.74	6.78 – 14.0	28.56	1.17	26.03 – 30.11	0.65	0.24	0.4 – 1.3
	2	11.53	1.54	7.47 – 13.47	29.18	0.5	28.66 – 30.48	1.37	0.49	0.4 – 1.8
	3	9.32	3.25	5.52 – 14.8	29.72	1.59	26.07 – 31.11	0.48	0.14	0.3 – 0.7
August	1	16.74	1.01	14.49 – 17.92	25.27	2.07	20.8 – 27.76	0.57	0.2	0.2 – 1.0
	2	14.79	2.67	6.74 – 16.41	26.98	1.14	25.8 – 30.0	1.52	0.78	0.4 – 2.9
	3	11.72	2.99	5.18 – 14.33	29.16	1.01	27.28 – 30.98	0.27	0.24	0.0 – 0.7
September	1	16.37	0.24	16.02 – 16.9	24.45	3.43	17.64 – 28.06	0.63	0.27	0.3 – 1.1
	2	15.91	0.49	15.16 – 16.58	27.25	0.4	26.52 – 27.74	1.12	0.53	0.4 – 1.8
	3	15.97	0.69	15.3 – 17.02	25.29	2.11	21.58 – 27.38	0.48	0.17	0.3 – 0.8
October	1	6.95	0.24	6.57 – 7.27	25.46	2.45	20.02 – 30.05	1.97	0.56	1.1 – 3.0
	2	6.64	0.18	6.31 – 6.87	27.61	1.2	25.41 – 29.78	2.3	0.71	1.3 – 3.4
	3	6.87	0.39	6.24 – 7.33	28.56	0.88	27.0 – 29.57	0.95	0.24	0.6 – 1.2

515

Month	Zone	Fluorescence (mg/m³)			PAR (µEinst/s/m²)		
		Mean	SD	Range	Mean	SD	Range
May	1	0.3	0.14	0.12 – 0.55	778.94	440.04	55.69 – 1733.92
	2	0.38	0.17	0.08 – 0.62	1218.98	1006.02	26.82 – 3217.33
	3	0.48	0.11	0.38 – 0.68	825.48	528.99	33.24 – 1626.41
June	1	0.94	0.48	-0.07 – 1.49	1883.33	379.99	1285.7 – 2655.6
	2	1.56	0.57	0.65 – 2.2	1666.97	543.02	868.45 – 2390.6
	3	0.87	0.27	0.51 – 1.27	626.15	572.52	80.83 – 1438.0
July	1	0.33	0.18	0.0 – 0.63	1050.57	619.66	143.93 – 2343.7
	2	0.57	0.24	0.27 – 1.14	550.39	181.17	332.92 – 922.06
	3	0.85	0.28	0.24 – 1.13	468.83	300.57	155.1 – 1049.8
August	1	0.67	0.36	0.06 – 1.34	1478.43	657.78	179.69 – 2310.3
	2	0.61	0.19	0.27 – 0.94	1878.56	491.86	1267.5 – 2634.6
	3	0.31	0.12	0.14 – 0.53	1879.65	549.2	1063.0 – 2639.4
September	1	2.08	0.99	1.14 – 4.06	450.02	178.31	235.64 – 769.47
	2	1.21	0.46	-0.03 – 1.86	230.75	207.38	41.12 – 667.43
	3	1.14	0.19	0.91 – 1.37	208.95	112.16	87.5 – 372.87

October	1	1.21	0.23	0.89 – 1.71	683.57	309.53	315.77 – 1347.9
	2	0.89	0.27	0.57 – 1.42	150.15	120.83	58.16 – 426.24
	3	1.2	0.27	0.95 – 1.79	345.38	238.19	127.78 – 876.06

Table A3: Mean (\pm SD) depth of the thermocline, halocline, pycnocline, euphotic zone, and subsurface fluorescence maxima (Sub. fluor. max.), and mean stratification index, by the three site zones and sampling month.

Month	Zone	Thermocline (m)	Halocline (m)	Pycnocline (m)	Euphotic Zone (m)	Sub. fluor. max. (m)	Stratification Index (kg/m^3)
May	1	4.2 (1.1) – 5.0 (1.3)	3.7 (0.4) – 4.7 (1.2)	3.7 (0.4) – 4.7 (1.2)	11.0 (3.9)	4.0 (/)	3.6 (1.9)
	2	3.7 (0.4) – 4.0 (0.8)	3.6 (0.4) – 4.4 (1.2)	3.7 (0.4) – 4.2 (0.8)	12.6 (4.9)	11.0 (/)	4.0 (2.4)
	3	3.5 (0.0) – 5.8 (2.1)	3.5 (0.0) – 5.1 (1.1)	3.5 (0.0) – 4.8 (1.1)	9.2 (3.2)	/	7.8 (2.2)
June	1	12.0 (7.7) – 13.0 (8.5)	14.0 (7.7) – 14.5 (7.9)	15.1 (8.1) – 15.7 (8.2)	8.5 (1.6)	5.6 (5.1)	3.2 (1.5)
	2	14.9 (9.9) – 16.1 (9.2)	5.3 (2.9) – 10.9 (7.3)	5.7 (2.8) – 10.9 (7.3)	6.8 (2.1)	3.3 (0.6)	2.0 (1.2)
	3	13.8 (13.8) – 15.2 (15.3)	20.5 (15.6) – 20.5 (15.6)	20.0 (16.3) – 21.0 (16.3)	12.1 (2.5)	4.2 (2.5)	1.8 (1.5)
July	1	5.2 (2.0) – 11.3 (4.6)	5.5 (2.1) – 8.6 (4.7)	5.0 (2.1) – 8.5 (4.2)	20.8 (0.4)	12.5 (5.2)	2.7 (1.3)
	2	4.1 (1.3) – 14.7 (6.3)	6.2 (1.5) – 8.8 (2.5)	4.8 (1.8) – 7.2 (2.5)	18.6 (4.3)	12.8 (6.3)	2.3 (0.9)
	3	5.3 (2.2) – 15.3 (3.8)	6.8 (1.5) – 8.2 (1.5)	5.7 (1.9) – 7.5 (2.9)	19.4 (2.6)	14.9 (3.5)	2.1 (1.5)
August	1	6.1 (1.3) – 13.2 (4.7)	6.5 (3.0) – 11.9 (5.0)	6.0 (1.8) – 11.3 (3.1)	16.1 (3.4)	5.5 (1.8)	5.5 (2.0)
	2	6.5 (6.4) – 14.3 (5.2)	4.1 (1.4) – 11.9 (4.1)	4.1 (1.4) – 11.8 (3.9)	11.8 (2.3)	4.5 (1.2)	3.9 (2.0)
	3	7.5 (6.9) – 12.2 (5.6)	7.8 (7.2) – 11.2 (6.2)	7.8 (7.2) – 9.2 (6.4)	20.6 (2.1)	10.6 (3.4)	2.8 (1.2)
September	1	9.5 (2.0) – 14.2 (4.1)	4.7 (2.6) – 11.8 (4.2)	6.0 (3.4) – 12.1 (4.1)	17.7 (2.7)	/	5.3 (2.7)
	2	11.2 (4.5) – 17.4 (6.5)	10.3 (4.5) – 12.8 (3.3)	11.4 (4.6) – 13.8 (3.1)	14.3 (3.0)	5.3 (2.5)	2.6 (2.1)
	3	5.5 (2.1) – 14.9 (6.8)	5.2 (2.1) – 7.6 (2.7)	5.6 (2.0) – 7.8 (2.6)	27.9 (2.3)	4.0 (1.4)	5.4 (2.1)
October	1	/	3.5 (0.0) – 4.0 (0.5)	3.5 (0.0) – 4.1 (0.5)	7.2 (1.3)	/	4.3 (1.9)
	2	/	4.5 (1.7) – 6.8 (1.5)	3.5 (0.0) – 4.5 (0.0)	9.6 (2.1)	/	2.3 (1.2)
	3	10.5 (/) – 10.5 (/)	8.5 (/) – 8.5 (/)	8.5 (/) – 8.5 (/)	11.7 (4.5)	/	1.9 (0.7)

520

525

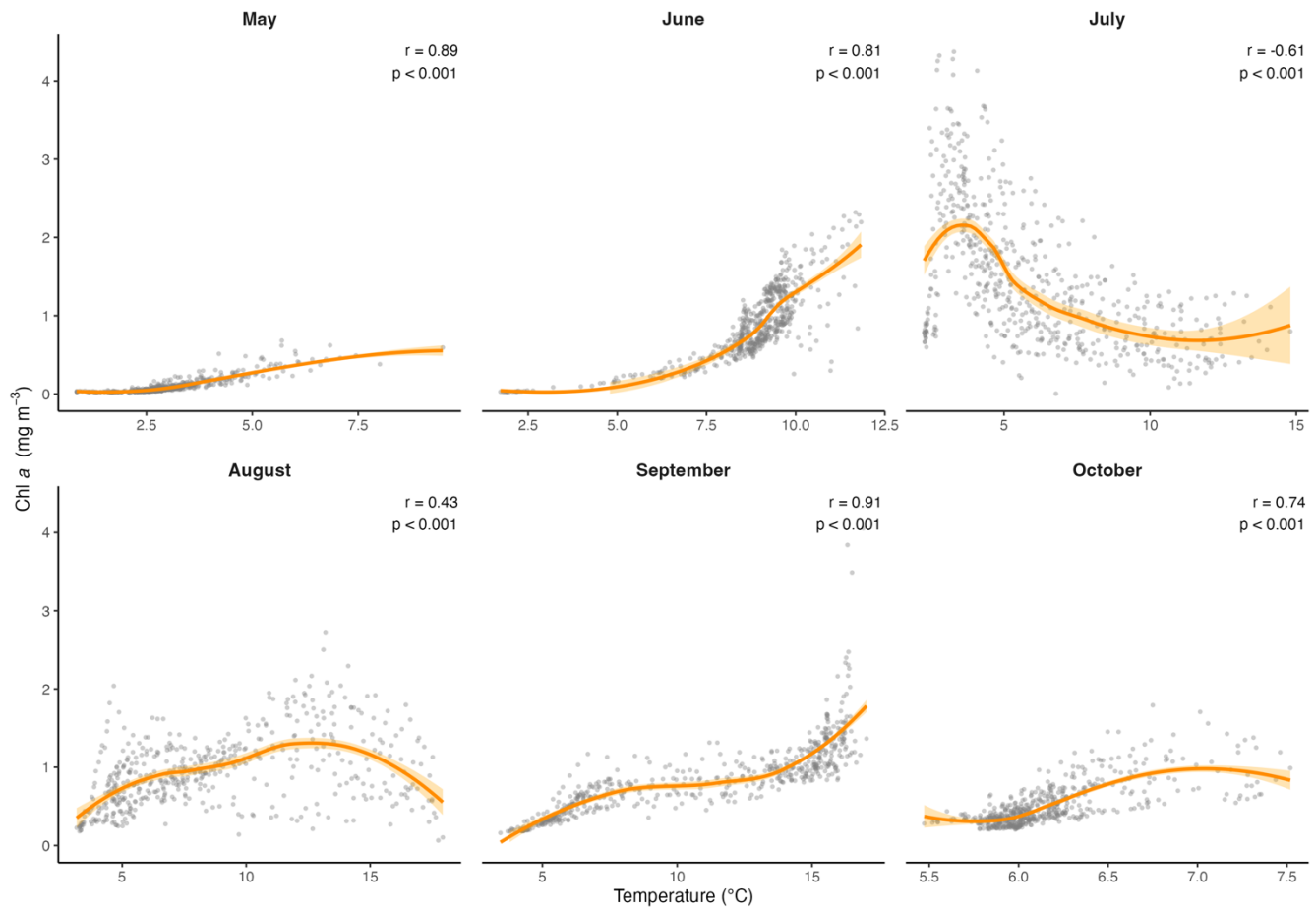


Figure A1: Scatter plots showing the monthly relationships between Chl *a* and temperature, across the transect. The orange line represents the LOESS curve with 95% confidence interval (shaded area). The Spearman correlation (r) and its p-value are also indicated.

530

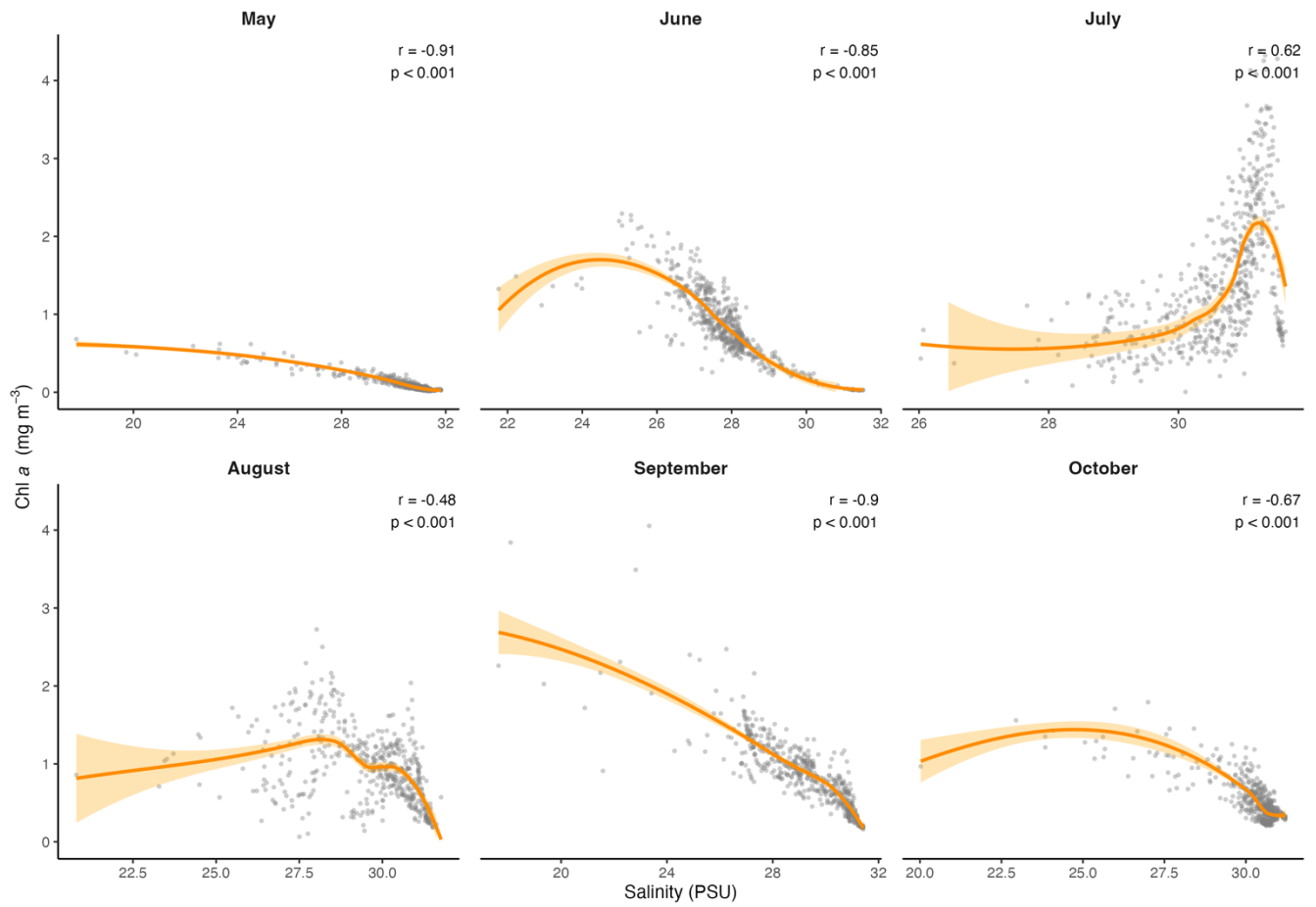


Figure A2: Scatter plots showing the monthly relationships between Chl *a* and salinity, across the transect. The orange line represents the LOESS curve with 95% confidence interval (shaded area). The Spearman correlation (*r*) and its *p*-value are also indicated.

535

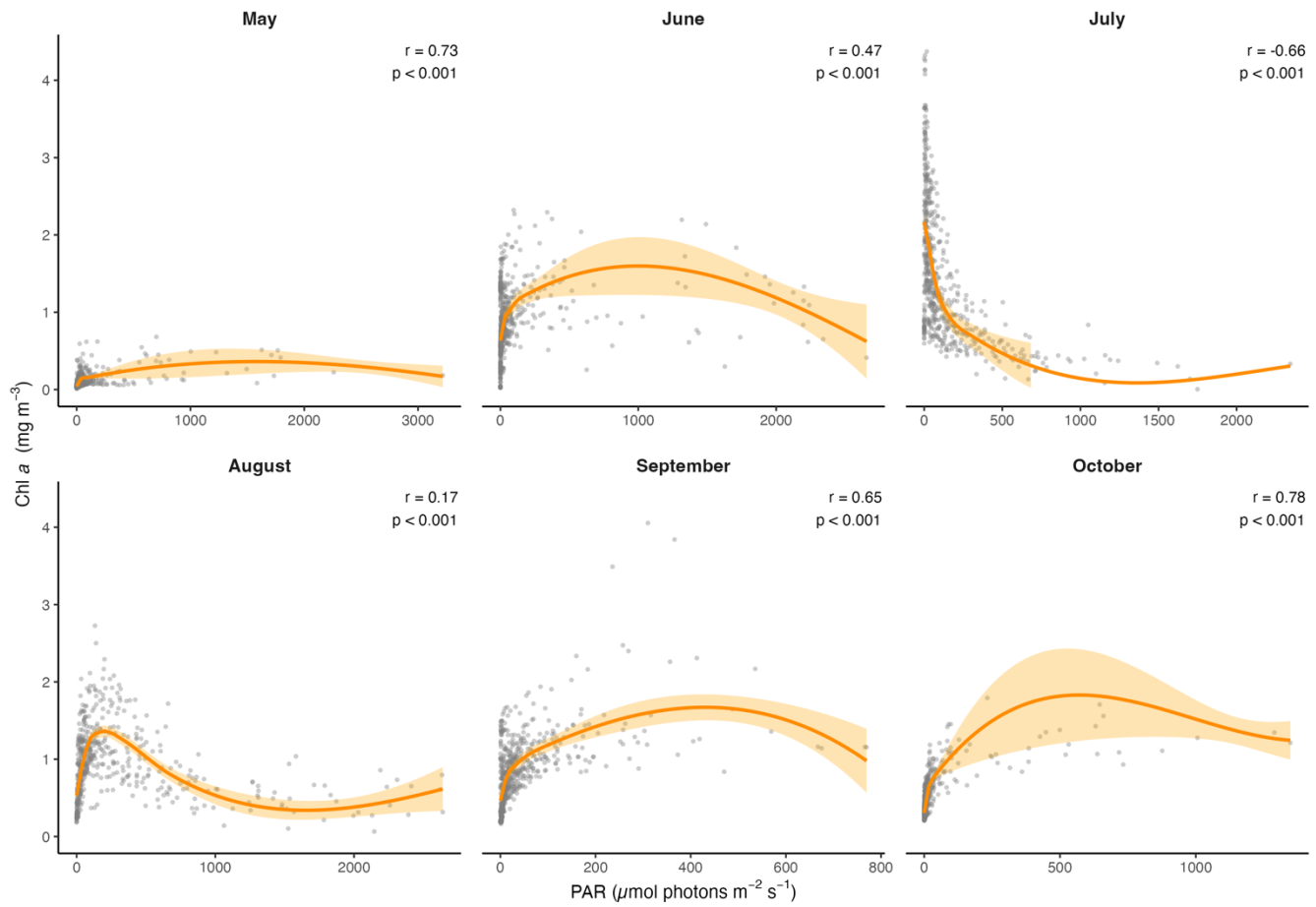


Figure A3: Scatter plots showing the monthly relationships between Chl *a* and PAR, across the transect. The orange line represents the LOESS curve with 95% confidence interval (shaded area). The Spearman correlation (*r*) and its *p*-value are also indicated.

540

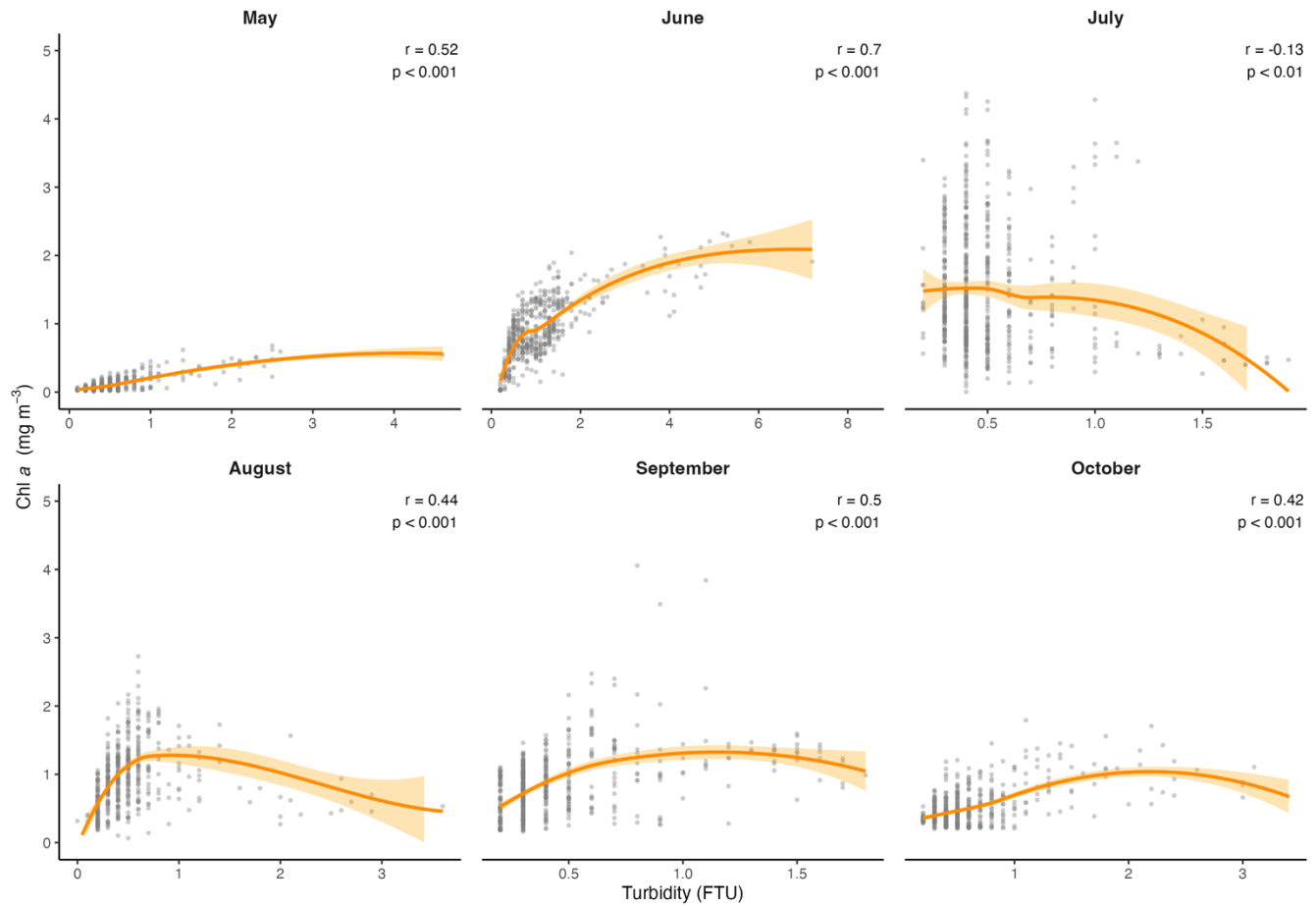


Figure A4: Scatter plots showing the monthly relationships between Chl *a* and turbidity, across the transect. The orange line represents the LOESS curve with 95% confidence interval (shaded area). The Spearman correlation (*r*) and its *p*-value are also indicated.

545

Author contribution

EA and ÉST worked on the conceptualization and the methodology of this study. EA performed the formal analysis and visualization. EA and ÉST wrote the original draft and JC and NJ revised the manuscript. ÉST and JC worked on the project administration and funding acquisition.

550

Competing interests

The authors declare that they have no conflict of interest.

Acknowledgments

This is scientific contribution to the Research Chair on Coastal Ecosystems and Port, Industrial and Maritime Activities (EcoZone Chair), a partnership between Université Laval, the Port of Sept-Îles (PSI), and the Northern Institute for Environmental and Occupational Health Research (INREST). We thank INREST for providing access to their premises, as well as to the laboratory and equipment on site. We thank Sabrina Allard, Louis-Joseph Brouillard, Lydiane Bélanger, and Marie-Christine Landry for their help with sampling. We also thank Québec-Océan (Université Laval) for its logistical and financial support, Sylvain Blondeau for his precious help in the field and Pascal Guillot for raw data processing. Finally, we thank Dermot Antoniadou, Paul Hamilton, ~~and~~ Ladd E. Johnson, and anonymous reviewers for their constructive comments, leading to the improvement of this manuscript.

References

- Allard, S.: Comprendre l'écosystème hivernal des zones portuaires subarctiques: le microbiome et les diatomées de la baie de Sept-Îles (Québec, Canada). M.S. thesis, Université Laval, Quebec, Canada, 2024.
- Allard, S., Gosselin, M., and Saulnier-Talbot, É.: Winter diatom assemblage composition to track shrinking seasonal sea ice cover in a coastal subarctic bay (Quebec, Canada), *Diatom Res.*, 1–20, <https://doi.org/10.1080/0269249X.2025.2534359>, 2025.
- Arseneault, E., Pienitz, R., Carrière, J., and Saulnier-Talbot, É.: Insights into Diatom Substrate Preferences in the Inter-Tidal Zone of a Subarctic Coast, *Hydrobiology*, 2, 537–553, <https://doi.org/10.3390/hydrobiology2040036>, 2023.
- Arseneault, E., and Saulnier-Talbot, É.: Snapshots of ice-free season dynamics in the near-shore water column of the northern Gulf of St. Lawrence, Canada, *Borealis*, V1 [data set], <https://doi.org/10.5683/SP3/ALRWON>, 2025a.
- Arseneault, E., and Saulnier-Talbot, É.: Species-environment relationships of coastal diatoms from the Sept-Îles region, Gulf of St. Lawrence (Québec, Canada), *J. Phycol.*, <https://doi.org/10.1111/jpy.70094>, 2025b.
- Araújo, C. A. S., Belzile, C., Tremblay, J.-É., and Bélanger, S.: Environmental niches and seasonal succession of phytoplankton assemblages in a subarctic coastal bay: Applications to remote sensing estimates, *Front. Mar. Sci.*, 9, 1001098, <https://doi.org/10.3389/fmars.2022.1001098>, 2022.
- Aubut Demers, K., Le Hénaff, A. and Carrière, J.: État des glaces, in: *Observatoire Environnemental de la Baie de Sept-Îles*, edited by: Carrière, J., INREST, Sept-Îles, QC, Canada, 593–612, 2018.
- Beauchesne, D., Daigle, R. M., Vissault, S., Gravel, D., Bastien, A., Bélanger, S., Bernatchez, P., Blais, M., Bourdages, H., Chion, C., Galbraith, P. S., Halpern, B. S., Lavoie, C., McKindsey, C. W., Mucci, A., Pineault, S., Starr, M., Ste-Marie, A.-S., and Archambault, P.: Characterizing Exposure to and Sharing Knowledge of Drivers of Environmental Change in the St. Lawrence System in Canada, *Front. Mar. Sci.*, 7, <https://doi.org/10.3389/fmars.2020.00383>, 2020.
- Bélanger, L.: Analyse spatiale et temporelle de la diversité microbienne dans la Baie de Sept-Îles, QC, M.S.thesis, Université Laval, Quebec, Canada, 2024.

- 595 Blais, M., Galbraith, P.S., Plourde, S., Scarratt, M., Devine, L. and Lehoux, C.: Chemical and Biological Oceanographic Conditions in the Estuary and Gulf of St. Lawrence during 2017. DFO Can. Sci. Advis. Sec. Res. Doc. 2019/009. iv + 56 pp, 2019.
- 600 Bourque, M. and Kelley, D. E.: Evidence of wind-driven upwelling in Jacques-Cartier strait, *Atmos.-Ocean*, 33, 621–637, <https://doi.org/10.1080/07055900.1995.9649548>, 1995.
- Bourque, M., and Malouin, J.: Guide d'intervention en matière de conservation et de mise en valeur des habitats littoraux de la MRC de Sept-Rivières, Comité ZIP Côte-Nord du Golfe, Canada, 155 pp., 2009.
- 605 Browning, T. J. and Moore, C. M.: Global analysis of ocean phytoplankton nutrient limitation reveals high prevalence of co-limitation, *Nat. Commun.*, 14, 5014, <https://doi.org/10.1038/s41467-023-40774-0>, 2023.
- Carrière, J., and Dreujou, E: *Projet Pilote Enviro-Actions*, in : *Actes du Symposium Enviro-Actions*, edited by: INREST, 18, 2024.
- 610 Carrière, J., Le Hénaff, A., and Aubut Demers, K.A.: Qualité de l'eau, in: *Observatoire Environnemental de la Baie de Sept-Îles*, edited by: Carrière, J., INREST, Sept-Îles, QC, Canada, 83-211, 2018a.
- Carrière, J., Le Hénaff, A., and Aubut Demers, K.: Description du site d'étude, in: *Observatoire Environnemental de la Baie de Sept-Îles*, edited by: Carrière, J., INREST, Sept-Îles, QC, Canada, 45-82, 2018b.
- 615 Castagno, A. P., Wagner, T. J. W., Cape, M. R., Lester, C. W., Bailey, E., Alves-de-Souza, C., York, R. A., and Fleming, A. H.: Increased sea ice melt as a driver of enhanced Arctic phytoplankton blooming, *Global Change Biol.*, 29, 5087–5098, <https://doi.org/10.1111/gcb.16815>, 2023.
- 620 Cloern, J. E.: Turbidity as a control on phytoplankton biomass and productivity in estuaries. *Cont. Shelf Res.*, 1367-1381, 1987.
- Cloern, J. E.: Tidal stirring and phytoplankton bloom dynamics in an estuary, *J. Mar. Res.*, 49, 203–221, <https://doi.org/10.1357/002224091784968611>, 1991.
- 625 De Boyer Montégut, C., Madec, G., Fischer, A. S., Lazar, A., and Iudicone, D.: Mixed layer depth over the global ocean: An examination of profile data and a profile-based climatology, *J. Geophys. Res.*, 109, 2004JC002378, <https://doi.org/10.1029/2004JC002378>, 2004.
- 630 Díez-Minguito, M. and de Swart, H. E.: Relationships Between Chlorophyll-a and Suspended Sediment Concentration in a High-Nutrient Load Estuary: An Observational and Idealized Modeling Approach, *J. Geophys. Res.: Oceans*, 125, e2019JC015188, <https://doi.org/10.1029/2019JC015188>, 2020.
- 635 Doyon, P. and Ingram, R. G.: Seasonal upper-layer T–S structure in the Gulf of St. Lawrence during the ice-free months, *Deep Sea Res. II*, 47, 385–413, [https://doi.org/10.1016/S0967-0645\(99\)00112-5](https://doi.org/10.1016/S0967-0645(99)00112-5), 2000.
- Dreujou, E., McKindsey, C. W., Grant, C., Tréau de Coeli, L., St-Louis, R., and Archambault, P.: Biodiversity and Habitat Assessment of Coastal Benthic Communities in a Sub-Arctic Industrial Harbor Area, *Water*, 12, 2424, <https://doi.org/10.3390/w12092424>, 2020.
- 640 Ferrario, F., Araújo, C. A. S., Bélanger, S., Bourgault, D., Carrière, J., Carrier-Belleau, C., Dreujou, E., Johnson, L. E., Juniper, S. K., Mabit, R., McKindsey, C. W., Ogston, L., Picard, M. M. M., Saint-Louis, R., Saulnier-Talbot, É., Shaw, J.-L., Templeman, N., Therriault, T. W., Tremblay, J.-E., and Archambault, P.: Holistic environmental monitoring in ports as an

- 645 opportunity to advance sustainable development, marine science, and social inclusiveness, *Elem. Sci. Anth.*, 10, 00061, <https://doi.org/10.1525/elementa.2021.00061>, 2022.
- Fiedler, P. C.: Comparison of objective descriptions of the thermocline, *Limnol. Oceanogr. Methods*, 8, 313–325, <https://doi.org/10.4319/lom.2010.8.313>, 2010.
- 650 Fisheries and Ocean Canada, Sept-Îles-02780, <https://www.marees.gc.ca/fr/stations/02780> Last access: 15 December 2024.
- Galbraith, P. S.: Winter water masses in the Gulf of St. Lawrence, *J. Geophys. Res.: Oceans*, 111, <https://doi.org/10.1029/2005JC003159>, 2006.
- 655 Galbraith, P. S., Sévigny, C., Bourgault, D., and Dumont, D.: Sea Ice Interannual Variability and Sensitivity to Fall Oceanic Conditions and Winter Air Temperature in the Gulf of St. Lawrence, Canada, *J. Geophys. Res.: Oceans*, 129, e2023JC020784, <https://doi.org/10.1029/2023JC020784>, 2024a.
- 660 Galbraith, P. S., Blais, M., Lizotte, M., Cyr, F., Bélanger, D., Casault, B., Clay, S., Layton, C., Starr, M., Chassé, J., Azetsu-Scott, K., Coyne, J., Devred, E., Gabriel, C.-E., Johnson, C. L., Maillet, G., Pepin, P., Plourde, S., Ringuette, M., and Shaw, J.-L.: Oceanographic conditions in the Atlantic zone in 2023, *Can. Tech. Rep. Hydrogr. Ocean Sci.*, 379 pp., 2024b.
- Government of Canada: Données Historiques, Station Sept-Îles, https://climate.meteo.gc.ca/historical_data/search_historic_data_f.html, last access: 24 April 2025.
- 665 Government of Québec, ministère du Développement durable, de l'Environnement et des Parcs, Direction du patrimoine écologique et des parcs: Réserve écologique de la Matamec, Conservation Plan, 14 pp., 2011.
- IPCC: Sections, in: *Climate Change 2023: Synthesis Report. Contribution of Working Groups I, II and III to the Sixth Assessment Report of the Intergovernmental Panel on Climate Change*, edited by: Lee, H. and Romero, J., IPCC, Geneva, Switzerland, 35-115, <https://doi.org/10.59327/IPCC/AR6-9789291691647>, 2023.
- Janecki, M., Dybowski, D., Rak, D., and Dzierzbicka-Glowacka, L.: A New Method for Thermocline and Halocline Depth Determination at Shallow Seas, *J. Phys. Oce.*, 52, 2205–2218, <https://doi.org/10.1175/JPO-D-22-0008.1>, 2022.
- 675 Joshi, N., Montero-Serrano, J.-C., Lefebvre, C., and Saulnier-Talbot, É.: Tracking Pre- and Post-Industrialization Changes in the Bay of Sept-Îles, Canada, Using Foraminifera as Bioindicators, *Journal of Coastal Research*, 41, <https://doi.org/10.2112/JCOASTRES-24A-00009>, 2025.
- Kirk, J. T.: *Light and photosynthesis in aquatic ecosystems*. Cambridge University Press, 1994.
- 680 Laliberté, J. and Larouche, P.: Chlorophyll-a concentration climatology, phenology, and trends in the optically complex waters of the St. Lawrence Estuary and Gulf, *J. Mar. Syst.*, 238, 103830, <https://doi.org/10.1016/j.jmarsys.2022.103830>, 2023.
- 685 Lefebvre, C.: Évaluation du potentiel des pigments comme bioindicateurs de la diversité bactérienne et algale dans un milieu côtier anthropisé (Baie de Sept-Îles, Québec), M.S. thesis, Université Laval, Québec, 2023.
- Leppäranta, M., and Myrberg, K.: Topography and Hydrography of the Baltic Sea, in: *Physical Oceanography of the Baltic Sea*, Springer Praxis Books, Berlin, Heidelberg, 41-88, 2009.
- 690 Lim, A. S., Park, N. Y., Choi, H. S., Kang, S. U., Ok, J. H., and Yoo, Y. D.: Influence of environmental parameters on marine plankton diversity in the southern coastal waters of Korea: Emphasis on thermal stratification, *Mar. Environ. Res.*, 203, 106829, <https://doi.org/10.1016/j.marenvres.2024.106829>, 2025.

- 695 Liu, B., De Swart, H. E., and De Jonge, V. N.: Phytoplankton bloom dynamics in turbid, well-mixed estuaries: A model study, *Estuarine, Coast. Shelf Sci.*, 211, 137–151, <https://doi.org/10.1016/j.ecss.2018.01.010>, 2018.
- 700 Long, Z., Perrie, W., Chassé, J., Brickman, D., Guo, L., Drozdowski, A., and Hu, H.: Impacts of Climate Change in the Gulf of St. Lawrence, *Atmos.-Ocean*, 54, 337–351, <https://doi.org/10.1080/07055900.2015.1029869>, 2016.
- [Lund-Hansen, L. C.: Diffuse attenuation coefficients \$K_d\$ \(PAR\) at the estuarine North Sea–Baltic Sea transition: time-series, partitioning, absorption, and scattering, *Estuar. Coast. Shelf Sci.*, 61, 251–259, <https://doi.org/10.1016/j.ecss.2004.05.004>, 2004.](https://doi.org/10.1016/j.ecss.2004.05.004)
- 705 Maske, H., Ochoa, J., Almeda-Jauregui, C. O., Ruiz-de la Torre, M. C., Cruz-López, R., and Villegas-Mendoza, J. R.: Near-surface temperature gradient in a coastal upwelling regime, *J. Geophys. Res.: Oceans*, 119, 4972–4982, <https://doi.org/10.1002/2014JC010074>, 2014.
- 710 May, C. L., Koseff, J. R., Lucas, L. V., Cloern, J. E., and Schoellhamer, D. H.: Effects of spatial and temporal variability of turbidity on phytoplankton blooms, *Mar. Ecol. Prog. Ser.*, 254, 111-128, 2003.
- Nielsen, J. M., Sigler, M. F., Eisner, L. B., Watson, J. T., Rogers, L. A., Bell, S. W., Pelland, N., Mordy, C. W., Cheng, W., Kivva, K., Osborne, S., and Stabeno, P.: Spring phytoplankton bloom phenology during recent climate warming on the Bering Sea shelf, *Prog. Oceanogr.*, 220, 103176, <https://doi.org/10.1016/j.pocean.2023.103176>, 2024.
- 715 Paquette, L., Le Hénaff, A., and Carrière, J.: Courants Marins, in: Observatoire Environnemental de la Baie de Sept-Îles, edited by: Carrière, J., INREST, Sept-Îles, QC, Canada, 571-588, 2018.
- 720 Pärn, O., Friedland, R., Rjazin, J., and Stips, A.: Regime shift in sea-ice characteristics and impact on the spring bloom in the Baltic Sea, *Oceanol.*, 64, 312–326, <https://doi.org/10.1016/j.oceano.2021.12.004>, 2022.
- Port of Sept-Îles: <https://www.portsi.com/port/>, last access: 02 January 2025.
- 725 R Core Team: R: A language and environment for statistical computing, R Foundation for Statistical Computing, Vienna, Austria, <https://www.R-project.org/>, 2022.
- Roden, C.M., and Raine, R.: Phytoplankton Blooms and a Coastal Thermocline Boundary along the West Coast of Ireland, *Estuar. Coast. Shelf Sci.*, 39, 511-526, 1994.
- 730 Roegner, G. C., Seaton, C., and Baptista, A. M.: Climatic and Tidal Forcing of Hydrography and Chlorophyll Concentrations in the Columbia River Estuary, *Estuaries and Coasts*, 34, 281–296, <https://doi.org/10.1007/s12237-010-9340-z>, 2011.
- Shaw, J.-L., ~~Bourgault, D., and Dumont, D.~~: Hydrodynamique de la Baie de Sept-Îles, M.S. thesis, Université du Québec à Rimouski, Rimouski, QC, Canada, 2019.
- 735 Shaw, J.-L., Bourgault, D., Dumont, D., and Lefavre, D.: Hydrodynamics of the Bay of Sept-Îles, *Atmos.-Ocean*, 10, 1–17, <https://doi.org/10.1080/07055900.2022.2141605>, 2022.
- 740 Stramska, M. and Jakacki, J.: Variability of chlorophyll a concentration in surface waters of the open Baltic Sea, *Oceanol.*, 66, 365–380, <https://doi.org/10.1016/j.oceano.2024.02.003>, 2024.
- Wang, D., Kuang, C., Wang, G., Liu, J., Song, W., Xing, R., and Zou, Q.: Factors Influencing the Spatio-Temporal Distribution of Chlorophyll-a in Jinmeng Bay, China, *J. Mar. Sci. Eng.*, 12, 384, <https://doi.org/10.3390/jmse12030384>, 2024.

- 745 Wei, X. and Zhao, H.: Spatiotemporal distribution of chlorophyll-*a* concentration in the south China sea and its possible environmental regulation mechanisms, *Mar. Environ. Res.*, 204, 106902, <https://doi.org/10.1016/j.marenvres.2024.106902>, 2025.
- 750 Winslow, L., Read, J., Woolway, R., Brenttrup, J., Leach, T., Zwart, J., Albers, S., and Collinge, D: `rLakeAnalyzer`: Lake Physics Tools. R package version 1.11.4.1, <https://CRAN.R-project.org/package=rLakeAnalyzer>, 2019.
- 755 Wu, Y.-L., Zhou, C.-X., and Zhang, Y.-S.: Vertical Profiles of Chl-*a* and Primary Productivity in the Middle Continental Shelf Area and Eddy Area of the East China Sea, *Chin. J. Ocean. Limnol*, 20, 74–80, <https://doi.org/10.1007/BF02846614>, 2002.
- 755 Yasunaka, S., Ono, T., Sasaoka, K., and Sato, K.: Global distribution and variability of subsurface chlorophyll *a* concentrations, *Ocean Sci.*, 18, 255–268, <https://doi.org/10.5194/os-18-255-2022>, 2022.